Earth-Science Reviews 270 (2025) 105230

Contents lists available at ScienceDirect

Earth-Science Reviews

journal homepage: www.elsevier.com/locate/earscirev

Production and significance of Reactive Oxygen Species in the subsurface

Peng Zhang [a], Chiheng Chu [b], Xiaochuang Bu [c], Man Tong [a], Hong Wang [a], Yingxiao Tian [a], Hailiang Dong [d], Dongmei Zhou [e], Andreas Kappler [f], Philippe Van Cappellen [c], T. David Waite [g], Songhu Yuan [a,*]

[a] State Key Laboratory of Geomicrobiology and Environmental Changes, China University of Geosciences, Wuhan 430078, PR China
[b] Faculty of Agriculture, Life, and Environmental Sciences, Zhejiang University, Hangzhou 310058, PR China
[c] Ecohydrology Research Group, Department of Earth and Environmental Sciences, University of Waterloo, Waterloo, ON N2L 3G1, Canada
[d] Center for Geomicrobiology and Biogeochemistry Research, State Key Laboratory of Biogeology and Environmental Geology, China University of Geosciences, Beijing 100083, PR China
[e] State Key Laboratory of Pollution Control & Resource Reuse, School of the Environment, Nanjing University, Nanjing 210023, PR China
[f] Department of Geoscience, University of Tübingen, Tübingen 72074, Germany
[g] School of Civil and Environmental Engineering, University of New South Wales, Sydney, NSW 2052, Australia

ARTICLE INFO

Keywords:
Reactive oxygen species
Subsurface
Organic carbon decomposition
Contaminant transformation
Biogeochemical processes

ABSTRACT

Reactive oxygen species (ROS) play a crucial role in greenhouse gas emissions, nutrient and contaminant transformations, microbial dynamics and a range of biogeochemical processes in surficial environments including the atmosphere, surface waters, and oceans. In recent years, research in ROS has extended to the subsurface, hence, moving from predominantly photic, oxic and homogeneous environments into aphotic, anoxic and heterogeneous environments. In this review, we discuss the production mechanisms and significance of ROS in the subsurface. Production hotspots of ROS occur where O_2 is brought into contact with reduced species like ferrous iron and natural organic matter, hence creating thermodynamically unstable conditions. The time and space window for ROS production is therefore co-regulated by the reaction kinetics between O_2 and reduced species, with the latter acting as both ROS generators and consumers of long-lived ROS such as hydrogen peroxide (H_2O_2) and short-lived ROS such as hydroxyl radicals (•OH). The quantitative description of ROS cycling in subsurface environments is still in its early stages, however. Modeling of a pulsed groundwater O_2 intrusion yields the rates of •OH and H_2O_2 production of 0.003–0.049 and 0.09–2.52 mmol/h/kg dry soil/sediment, respectively. Advances in ROS analysis, footprint mapping and reactive transport modeling, as well as new knowledge about the molecular mechanisms of ROS production and cycling, would enable a more comprehensive assessment of the significance of ROS in subsurface biogeochemistry that, in turn, could benefit their potential applications, for example, in contaminant remediation strategies.

Contents

* Corresponding author.
E-mail address: yuansonghu622@cug.edu.cn (S. Yuan).

https://doi.org/10.1016/j.earscirev.2025.105230
Received 23 September 2024; Received in revised form 26 June 2025; Accepted 23 July 2025
Available online 23 July 2025

1. Introduction

Molecular O_2 (21 % *v*/v in air) and H_2O are the most abundant O-containing chemicals in the environment. These entities are relatively inert in their own right but can become highly reactive when they are transformed to so-called "reactive oxygen species" (ROS) via reduction and oxidation (redox) reactions (Taverne et al., 2018). Superoxide ($^{\bullet}O_2^-$), hydrogen peroxide (H_2O_2) and hydroxyl radicals ($^{\bullet}OH$) are the main ROS produced from partial O_2 reduction or H_2O oxidation. Because of their high reactivity, ROS play important roles in a wide range of environmental and biological systems (Diaz et al., 2013; Gligorovski et al., 2015). ROS were first discovered in the atmosphere, but the research focuses subsequently moved to biological system because of the significance of ROS to disease initiation and progression (Finkel and Holbrook, 2000; Hansel and Diaz, 2021). For example, ROS participate in the critical processes of cellular differentiation and signal transduction, and can oxidatively damage key cellular building blocks such as like nucleic acids and proteins (Finkel and Holbrook, 2000; Halliwell, 2024; Schieber and Chandel, 2014). In the environment, ROS can oxidize or degrade CH_4, NO_x and volatile organic compounds in the troposphere (Gligorovski et al., 2015; Savee et al., 2015), with $^{\bullet}OH$ recognized to be the dominant oxidant which determines the oxidizing capacity of the atmosphere (Gligorovski et al., 2015; Prinn et al., 2001). While their presence has been recognized for some time (Waite et al., 1988; Zika et al., 1993), there has been renewed interest in recent years in the presence of ROS in surface waters and shallow seawaters (Andrews et al., 2000; Mopper and Zhou, 1990), with increasing recognition of the significance of ROS in redox-sensitive substance transformation and microbial survival (Dong et al., 2021; Swanner et al., 2015; Tolar et al., 2016).

As these environments are photic, ROS production was initially considered to be driven by photochemical reactions involving inorganic compounds (e.g., NO_x) and organic photosensitizers (e.g., natural organic matter (NOM)) (Andrews et al., 2000; Mopper and Zhou, 1990; Waite et al., 1988). For instance, NOM can be excited by absorption of photons under sunlight irradiation, which leads to the production of a series of ROS through energy or electron transfer (Garg et al., 2011; Szymczak and Waite, 1991; Zheng et al., 2023). However, ROS have been later found in aphotic environments such as deep brackish and freshwater ponds as a result of extracellular reduction of O_2 by microbes including macrophytic plankton and particle-associated heterotrophic bacteria (Diaz et al., 2013; Rose et al., 2005; Zhang et al., 2016b). In the marine, dark extracellular $^{\bullet}O_2^-$ production by microbes represents a previously unconsidered global oxygen flux and sink comparable in magnitude to other processes, being estimated to comprise about a third of marine gross O_2 production (Sutherland et al., 2020). Extracellular H_2O_2 production in natural fresh waters and marine systems has been reported to occur through both the disproportionation or reduction of biologically or photochemically derived $^{\bullet}O_2^-$ as well as directly by other biological pathways (Garg et al., 2011; Hansel and Diaz, 2021; Hopwood et al., 2017; Rose et al., 2008a; Rose et al., 2008b; Zhang et al., 2016b). H_2O_2 has been recognized as a precursor of $^{\bullet}OH$, but less is known about the production of $^{\bullet}OH$ by microbial biota in dark environments (Schneider et al., 2016; Zinser, 2018).

Different from surface environments, subsurface environments are normally dark, anoxic or O_2-limited, and composed of a solid matrix with pores/fractures filled with fluid. This difference could be the reason that the role of ROS in subsurface environments has not been recognized until relatively recently (Dong et al., 2023; Page et al., 2013; Tong et al., 2016; Yu et al., 2024; Yuan et al., 2017). As the environment gradually transitions from surface to subsurface, aerobic heterotrophic bacteria becomes more difficult to survive and the abundance of reduced species increases (Tong et al., 2016; Trusiak et al., 2018; Zhang et al., 2024a). Because of the unique reductive characteristics of the subsurface environments, the mechanisms of ROS production differ from those in surface environments. When the reducing conditions in the subsurface are

disturbed by O_2, for example, the alternation of oxic and anoxic conditions due to water table fluctuations, reduction of O_2 by the reduced species present contributes to the production of ROS (Du et al., 2021; Page et al., 2013; Tong et al., 2016; Yu et al., 2021). Reduced iron-bearing clay minerals and reduced NOM are important components for ROS production in soils and sediments (Page et al., 2013; Tong et al., 2016; Liao et al., 2019). Extensive studies have documented the impact of dark ROS production on substance transformation and biogeochemical processes (Chen et al., 2021b; Tong et al., 2016). Thus, biotic and abiotic processes under dark subsurface conditions replace photochemical processes in the surface environment as the primary mechanisms for ROS production (Dai et al., 2022; Liu et al., 2024b). The contributions of biotic and abiotic mechanisms to ROS production depend on the biogeochemical characteristics of sediments/soils, O_2 availability, and external environmental conditions (such as climate and temperature) (Dai et al., 2022; Huang et al.,2023; Liu et al., 2024a; Zhang et al., 2024a; Zhao et al., 2022). Encouragingly, significant advancements have been made in terms of ROS quantification (Burns et al., 2012; Yu et al., 2024; Yuan et al., 2017), ROS production mechanisms (Chen et al., 2022a; Hansel and Diaz, 2021; Tong et al., 2016), ROS production in different redox-dynamic scenarios (Chen et al., 2021a; Tong et al., 2016; Yuan et al., 2017), and impact of ROS on contaminant attenuation and elemental cycling (Schaefer et al., 2017; Van Erk et al., 2023; Zeng et al., 2017).

As ROS in the subsurface are a relatively new research frontier, the following questions remain unanswered: (1) which species in the subsurface are effective in activating O_2 or splitting H_2O with resultant generation of ROS; (2) what conditions and scenarios are favorable for ROS production in the subsurface; (3) which methods can be used for ROS measurement under particular subsurface conditions; (4) what is the role of ROS in redox-sensitive substance transformation; and (5) how can both the rate of ROS production and the contribution of ROS to redox-sensitive substance transformation be quantified. Without a clear understanding of the answers to these questions, we cannot fully understand how and to what extent ROS can be produced in the subsurface and influence the transformation of redox-sensitive elements and contaminants. In this review, we first summarize recent progress in understanding of the production mechanisms and approaches to measurement of ROS in the subsurface. In order to advance the development of this new research frontier, we further provide i) guidelines for evaluating ROS production efficiency from different contributors, ii) the time and space windows appropriate to identifying ROS production hotspots in different scenarios, iii) the recommendations for choosing ROS measurement methods for different purposes, and iv) the kinetics and reactive transport models appropriate to quantifying ROS production and their relative contributions. Finally, we also provide advice on future research needs related to ROS generation in subsurface environments. The issues that we provided are important and have not been comprehensively reported before.

2. ROS Production Mechanisms in the Subsurface

2.1. General Pathways of ROS Production

ROS can, in principle, be generated by two contrasting processes in the subsurface. One process involves the reduction of O_2 to intermediate species via 1 or 2 electron redox processes (eqs. (1)–(4)) rather than the 4 electron reduction of O_2 to H_2O (eq. (5)) (Taverne et al., 2018). One-electron reduction of O_2 to $^{\bullet}O_2^-$ is thermodynamically unfavorable under standard (oxic) condition ($E^0 = -0.33$ V, Fig. 1a) but is favorable in natural waters as the steady-state concentrations of $^{\bullet}O_2^-$ and dissolved O_2 are in the pM–nM range (Hansel et al., 2015) and ~ 0.25 mM, respectively (E = 0.17–0.26 V). $^{\bullet}O_2^-$ tends to transform to H_2O_2 via a one electron reduction reaction ($E^0 = 1.72$ V, Fig. 1a). Another pathway for H_2O_2 generation is the two-electron reduction of O_2, which is thermodynamically favorable ($E^0 = 0.695$ V, Fig. 1a). As the dissociation energy of the O—O bond is 146 kJ/mol (Schoonen et al., 2006), H_2O_2 is relatively stable with a lifetime from hours to days (Hansel and Diaz, 2021). When activated by redox active species (including redox-active metals and reduced natural organic matter, etc.) in the subsurface, H_2O_2 transforms to $^{\bullet}OH$ ($E^0 = 2.73$ V, Fig. 1a), which is the most powerful oxidant in natural environments (Gligorovski et al., 2015).

$$O_2 + e^- \rightarrow O_2^{\cdot -} \quad E^0 = -0.33\ \text{V} \tag{1}$$

$$O_2^{\cdot -} + e^- + 2H^+ \rightarrow H_2O_2 \quad E^0 = 1.72\ \text{V} \tag{2}$$

$$O_2 + 2e^- + 2H^+ \rightarrow H_2O_2 \quad E^0 = 0.695\ \text{V} \tag{3}$$

$$H_2O_2 + e^- + H^+ \rightarrow \dot{O}H + H_2O \quad E^0 = 0.8\ \text{V} \tag{4}$$

$$O_2 + 4e^- + 4H^+ \rightarrow 2H_2O \quad E^0 = 1.23\ \text{V} \tag{5}$$

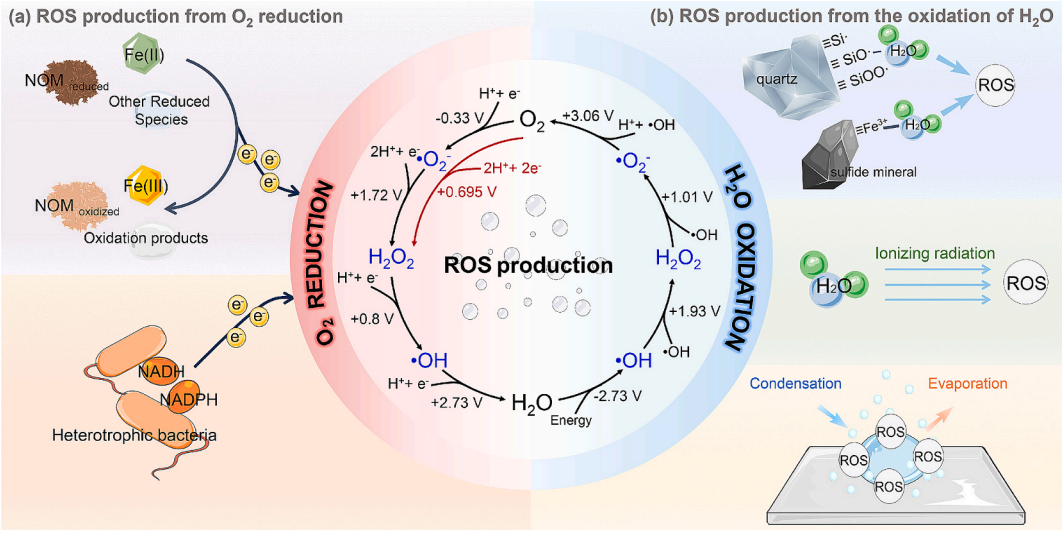

Fig. 1. Two pathways of ROS production in the subsurface. (a) ROS production from O_2 reduction, where O_2 is reduced to $^{\bullet}O_2^-$ and H_2O_2 by reduced species, such as Fe(II) and reduced NOM or extracellularly secreted NADH/NADPH. The standard reduction potentials of O_2 and each ROS are cited from the reference (Wood, 1988). (b) ROS production from H_2O oxidation, where H_2O is oxidized by the defect sites on mineral surface, by ionizing radiation, or by the strong electric field at the water-air interface of microdroplets.

Table 1
Summary of electron utilization efficiencies (EUE) for •OH production during oxygenation of different reduced species in soils and sediments.

Reduced species	pH	EUE for •OH production [a]	•OH yield from H_2O_2 decomposition [b]	References
Dissolved Fe(II)				
Fe^{2+}	6.0–8.0	0.4–2.9 %	0.7–5.2 %	(Hu et al., 2022; Qian et al., 2019; Zeng et al., 2019)
Fe(II)-phosphate	6.8	<5.1 %[d]	1.7 %	(Zeng et al., 2019)
Fe(II)-EDTA [c]	6.8	<42.3 %[d]	14.1 %	(Zeng et al., 2019)
Fe(II)-TPP [c]	6.8	<21 %[d]	7.0 %	(Zeng et al., 2019)
Fe(II)-NTA [c]	6.8	<44.1 %[d]	14.7 %	(Zeng et al., 2019)
Fe(II)-citrate$^-$	7.0	<30 %[d]	10.0 %	(Zhang and Yuan, 2017)
Fe(II)-HA [c]	7.0	1.2–2.8 %	4.3–6.3 %	(Zhang et al., 2022b)
Adsorbed Fe(II)				
Al_2O_3-Fe(II)	6.0	5.7–17.4 %	–[e]	(Chen et al., 2022b; Xie et al., 2020)
Fe(III) oxyhydroxides-Fe(II)	7.0–7.5	6.4 %	3.7 %	(Qian et al., 2019; Xie et al., 2020)
Montmorillonite-Fe(II)	7.5	7.5 %	–	(Xie et al., 2020)
Kaolinite-Fe(II)	7.5	12.3 %	–	(Xie et al., 2020)
Mineral structural Fe(II) [f]				
rNAu-2 [c]	6.0–7.5	6.0–27.3 %	2.3–8.8 %	(Yu et al., 2021a; Yuan et al., 2018; Zeng et al., 2017)
rSWy-2/−3 [c]	6.0	3.9–9.2 %	–	(Guo et al., 2021; Tong et al., 2016)
rIMt-2 [c]	6.0	1.7 %	–	(Guo et al., 2021)
rRAr-1 [c]	6.0	12.0 %	–	(Guo et al., 2021)
rISCz-1 [c]	6.0	2.5 %	–	(Guo et al., 2021)
Chlorite	7.0	18.0 %	–	(Tong et al., 2016)
Siderite	7.0	0.3–3.0 %	2.6 %	(Tong et al., 2016; Yu et al., 2021b)
Green rust	8.0	0.2 %	–	(Zhang et al., 2022a)
Pyrite	2.0–4.0	–	36–68 %	(Zhang et al., 2018)
Mackinawite	7.0	2.4–7.8 %	–	(Cheng et al., 2020; Cheng et al., 2016)
Fe(II) in soils/sediments				
Wetland sediment	7.0	1.4–2.7 %	–	(Xie et al., 2020; Zhang et al., 2023a; Zhao et al., 2021)
Paddy soil	7.0	0.9–2.7 %	–	(Chen et al., 2021a; Chen et al., 2021b)
Riparian sediment	7.0	0.9–3.0 %	–	(Zhang et al., 2024a; Zhang et al., 2023a)
Farmland sediment	7.0	1.7 %	–	(Xie et al., 2021)
Farmland sediment + EDTA/TPP [c]	7.0	3.2–14.1 %	–	(Xie et al., 2021)
Natural organic matters				
PPHA [c]	7.0	13.8 %	4.8 %	(Page et al., 2012)
AHA [c]	7.0	10.5–36 %	9.9 %–49.1 %	(Page et al., 2012; Yu et al., 2022; Yu et al., 2021a; Zhang et al., 2022b)
ESHA [c]	7.0	19.5 %	6.8 %	(Page et al., 2012)
Solid HA [c]	7.0	0.6–0.7 %	2.9 %	(Yu et al., 2022)
S(-II) and thiols				
S(-II) + oxidized NOM	7.0	2.4 %	–	(Niyuhire et al., 2022)
S(-II) + Fe(III) oxyhydroxides	7.0	1.1 %	–	(Niyuhire et al., 2019)
Thiols + natural siderite	7.0	1.4–2.0 %	–	(Yu et al., 2021b)
Thiols + Fe(III) oxyhydroxides	7.0	0.6–4.2 %	–	(Zhang et al., 2024b)

[a] The electron utilization efficiency (EUE) was calculated by eq. 10,
[b] The yield (Y) of •OH production from H_2O_2 decomposition was calculated by eq. 11
[c] EDTA, TPP and NTA represent ethylene diamine tetraacetate, tripolyphosphate and nitrilotriacetic acid, respectively; rNAu-2, rSWy-2/−3 and rIMt-2 represent the reduced forms of nontronite (NAu-2, iron-rich smectite), montmorillonite (SWy-2/−3, iron-poor smectite) and illite (IMt-2, as an illite end-member), respectively. rRAr-1 and rISCz-1 are the reduced mixed-layer smectite-illite, with smectite to illite ratios of 5:5 and 3:7, respectively. HA, PPHA, AHA and ESHA represent humic acid, Pahokee peat humic acid, Aldrich humic acid and Elliott soil humic acid, respectively.
[d] The EUE of those Fe(II) species for •OH production was estimated from the yield of •OH from H_2O_2 decomposition and the assumption that the efficiency of O_2 reduction to H_2O_2 was less than 100 %.
[e] The symbol "–" indicates that the data is not available.
[f] Some Fe(II) minerals (e.g., magnetite (Ardo et al., 2015)) and Fe(II)-containing soils/sediments (e.g., ref. (Chen et al., 2020; Schaefer et al., 2017)) have been reported to produce •OH. However, data on electron utilization efficiencies for •OH production and •OH yield from H_2O_2 decomposition are unavailable and thus are not included in the above table.

The opposite direction is the incomplete oxidation of H_2O to O_2 (eqs. (6)–(9), Fig. 1b). The first step is the transformation of H_2O to •OH (eq. (6)), which is thermodynamically unfavorable. ROS production by this pathway requires energy (Halliwell, 2006), which can be provided by the high-energy bonds in surface-defect sites of particular mineral surfaces under certain conditions (Borda et al., 2003; He et al., 2023) and ionizing radiation (Lefticariu et al., 2010). H_2O is first split to •OH and •H, and two •OH combines to H_2O_2, which further react with •OH to generate $\cdot O_2^-$ (Fig. 1b). In the subsurface, ROS production from O_2 reduction is the most important pathway, and the H_2O oxidation pathway only plays a role under specific conditions as detailed later.

$$H_2O \rightarrow \dot{O}H + H^+ + e^- \quad E^0 = -2.73\ V \qquad (6)$$

$$\dot{O}H + \dot{O}H \rightarrow H_2O_2\ E^0 = 1.93\ V \quad (7)$$

$$\dot{O}H + H_2O_2 \rightarrow \dot{O}_2 + H_2O + H^+\ E^0 = 1.01\ V \quad (8)$$

$$\dot{O}H + \dot{O}_2^- + H^+ \rightarrow O_2 + H_2O\ E^0 = 3.06\ V \quad (9)$$

$$EUE = 3 \times \frac{c_{\cdot OH}}{n\left(c_{0,rs}\text{-}c_{t,rs}\right)} \times 100\% \quad (10)$$

where $c_{\cdot OH}$ represents the cumulative concentration of •OH during oxygenation; $c_{0,\ rs}$ and $c_{t,\ rs}$ represent the concentrations of reduced species at the beginning and end, respectively; the variable n represents the number of electron release when reduced species was oxidized, giving the value of 1 for Fe(II), thiols and NOM and 2 for S(-II). As the reduction of O_2 to •OH requires 3 electrons, a coefficient of 3 was used.

$$Y = \frac{\Delta c_{\cdot OH}}{\Delta c_{H_2O_2}} \times 100\% \quad (11)$$

where $\Delta c_{\cdot OH}$ represents the cumulative concentration of •OH from H_2O_2 decomposition by reduced species; Δc_{H2O2} represents the consumption of H_2O_2 during reaction between H_2O_2 and reduced species.

2.2. Abiotic Mechanisms for ROS Production in the Subsurface

2.2.1. Abiotic Mechanisms for ROS Production from O_2 Reduction

Molecular O_2 is a paramagnetic biradical, with two unpaired electrons in two π^* orbitals within parallel spin. As most reductants cannot simultaneously donate two unpaired electrons within parallel spin to O_2, O_2 prefers to accept one electron at a time due to this spin restriction. Those reductants with unpaired electrons such as transition metals (e.g., Fe(II)) and organic radicals are thus appropriate for reducing O_2 to ROS (Krumova and Cosa, 2016). In the subsurface, Fe(II) and natural organic matter (NOM) are the most abundant reductants to satisfy this requirement.

(a) Fe(II). Iron is the most abundant transition metal element in the Earth's crust, with two main redox states: Fe(II) and Fe(III). The former in the subsurface exists as different species, including free (dissolved) Fe^{2+}, ligand-complexed Fe(II), surface-adsorbed Fe(II) on different minerals and solid matrixes, and structural Fe(II) in different minerals (Huang et al., 2021b). Fe(II) normally reduces O_2 to generate $\cdot O_2^-$, H_2O_2 and •OH sequentially (Rose and Waite, 2002). Almost all Fe(II) species can reduce O_2 to produce $\cdot O_2^-$ and H_2O_2, but only specific species can effectively decompose H_2O_2 to •OH (Remucal and Sedlak, 2011; Xie et al., 2020). The electron utilization efficiency (EUE) for •OH production from O_2 reduction by different Fe(II) species varies markedly from 0.4 % to <44.1 % (Table 1). Further, the EUE of Fe(II) in soils and sediments has been reported to be 0.9–3 % (Table 1), falling within this range. The exact reason for the striking influence of Fe(II) speciation on •OH production is not fully understood. The current understanding and knowledge can be roughly summarized as follows. In general, an outer-sphere mechanism preferentially generates •OH, while an inner-sphere mechanism preferentially generates high-valence iron with the relative proportions of the two mechanisms determining the yield of •OH (Remucal and Sedlak, 2011). For example, Fe(II) that is present as the aquated species $[Fe(H_2O)_6]^{2+}$ under acidic condition decomposes H_2O_2 to •OH at a high yield of nearly 100 %, while it transforms to $[Fe(OH)_x(H_2O)_{6\text{-}x}]^{(2\text{-}x)+}$ (x = 1–2) under pH-neutral condition and decomposes H_2O_2 to •OH at a low yield close to 0 (Remucal and Sedlak, 2011). In the subsurface, the yield of •OH from O_2 reduction is negatively related with the reactivity of Fe(II) species with O_2, that is, a faster reaction between an Fe(II) species and O_2 corresponded to a lower •OH yield (Xie et al., 2020). The reactivity of Fe(II) with O_2 is dependent on its coordination structure (Huang et al., 2021b; Miller et al., 2013), i.e., the electron-donating ability and the number of coordinated ligands. An electron-rich ligand (i.e., -OH for dissolved and surface adsorbed Fe(II)) increases Fe(II) reactivity but decreases •OH yield, while an electron-poor ligand (i.e., -OSi(VI) and -OFe(III) for mineral structural Fe(II)) functions contrarily (Xie et al., 2020). Based on this understanding, we can evaluate •OH production from Fe(II) species in subsurface matrices.

In analogous to Fe(II), manganese(II) (Mn(II)) can also reduce O_2 to generate ROS through the Haber-Weiss mechanism (Rosso and Morgan, 2002). However, due to both kinetic and thermodynamic factors, the abiotic oxidation of Mn(II) by O_2 is rather slow under circumneutral pH conditions (Morgan, 2005). In addition, the abundance of Mn(II) in soils and sediments is much lower than that of Fe(II). Hence, compared to Fe (II), the role of Mn(II) in ROS production may be minor.

(b) NOM. NOM in the subsurface has abundant functional groups with a wide range of reduction potentials. The electron accepting and donating capacities of NOM can reach the level of mol/kg (Aeschbacher et al., 2011; Klupfel et al., 2014). The redox activity is mainly attributed to quinone-like moieties (Ratasuk and Nanny, 2007). Reduced quinone moieties (i.e., semiquinones and hydroquinones) can reduce O_2 to $\cdot O_2^-$, H_2O_2 and •OH (Page et al., 2012). H_2O_2 production from the reaction of reduced NOM with O_2 has been recognized for a long time (Page et al., 2012), but •OH production via this pathway is not well understood. It is reported that NOM can decompose H_2O_2 to •OH at a high yield (tens of percent) (Yu et al., 2021a; Zhang et al., 2022b). It is likely that the reduced quinone moieties and/or redox active elements such as Fe that are present in NOM are responsible for the decomposition of H_2O_2 to •OH (Page et al., 2012). The electron utilization efficiencies for •OH production from O_2 reduction by dissolved and solid NOM are 10.5–36 % and 0.6–0.7 %, respectively (Table 1). This notable difference may be attributed to the higher yield of •OH production from H_2O_2 decomposition by dissolved NOM (Table 1). In addition, NOM may interact with Fe and influence ROS production as they commonly co-exist in the subsurface. NOM can form complexes with Fe(II)/Fe(III) and affect the yield of ROS production (Liu et al., 2024c; Zhang et al., 2022b). NOM can also react with Fe(II) by shuttling electrons from Fe(II) to O_2 (Yu et al., 2021a).

(c) Other Reduced Species. Other reduced species present in the subsurface include sulfide and organic thiols. The roles of these reductants in ROS production have been much less investigated because their concentrations are much lower than that of Fe(II) and NOM. These species are recognized to be able to reduce O_2 to $\cdot O_2^-$ and H_2O_2. However, reduction of O_2 by sulfide and thiols cannot effectively generate •OH (Niyuhire et al., 2022; Sun et al., 2020; Zhang et al., 2024b). Instead, the presence of Fe and NOM can largely increase H_2O_2 and •OH generation because of their catalytic role in mediating electron transfer from sulfide and thiols to O_2 (Niyuhire et al., 2019; Niyuhire et al., 2022; Sun et al., 2020). Electron transfer occurs initially from sulfide or thiols to Fe(III) minerals or NOM. The resulting Fe(II) or reduced NOM subsequently reduces O_2 to $\cdot O_2^-$, H_2O_2 and •OH. The electron utilization efficiencies for •OH production from O_2 reduction by sulfide and thiols are 1.1–2.4 % and 0.6–4.2 %, respectively (Table 1), which are consistent with those observed for Fe(II) and NOM.

2.2.2. Abiotic mechanisms for ROS production from H_2O oxidation

ROS production from H_2O oxidation in the subsurface has not been confirmed, but its occurrence is presumed likely. The high-energy bonds which can oxidize H_2O exist in the surface-defect sites of sulfidic minerals and quartz (Wu et al., 2023; Xia et al., 2023; Zhang et al., 2016a). As surface-defect sites may disappear when they are covered by solutes via adsorption, ROS production by this pathway is limited in the subsurface. It could be significant when surface-defect sites can be created by physical grinding due to tectonic activities (He et al., 2023; Stone et al., 2022). One notable example is the recent discovery of ROS production during quartz grinding (Wu et al., 2023), which points to a source of O_2 on early Earth (He et al., 2021; He et al., 2023). In addition to surface-defect sites, radiation emitted by the decay of radioactive elements such as uranium (^{238}U), thorium (^{232}Th), and potassium (^{40}K) can also dissociate water molecules to form ROS (Lefticariu et al., 2010).

Recent studies have reported the interesting finding that ROS is formed in micrometer-sized water droplets (microdroplets), likely due to the oxidation of water by the strong electric field at the water-air interface of these microdroplets (Lee et al., 2020; Lee et al., 2019; Pan et al., 2023). As the size of microdroplets increases, the ratio of surface area to volume decreases, leading to an anticipated decrease in ROS concentration due to the dilution effect (Lee et al., 2020; Lee et al., 2019). For instance, the concentration of H_2O_2 becomes negligible in droplets larger than 10 μm (Lee et al., 2020). Therefore, the formation of new microdroplets is crucial for ROS production. A typical example is that the cumulative concentration of ROS in microdroplets increases with prolonged evaporation and condensation (Pan et al., 2023). In addition, some studies have reported that the interaction between water molecules and the solid surfaces (e.g., SiO_2) may also lead to the production of ROS (Chen et al., 2022a; Lin et al., 2020; Nie et al., 2020; Xu et al., 2018). Specifically, when water molecules interact with a solid surface and their electron clouds overlap, the acidic hydroxyl groups (Si-OH) on SiO_2 surface may be ionized to generate hydronium cations and silanolate anions (Si—O) (Chen et al., 2022a). The later can further react with the excited water species of H_2O^+, thereby producing •OH (Chen et al., 2022a). The recombination of two •OH may subsequently form H_2O_2 (Chen et al., 2022a; Lee et al., 2020). These findings indicate ROS may be generated in the subsurface when new water microdroplets are formed or the water molecule interact with oxygen-containing groups on solid substrates. More field-related studies are warranted to justify ROS production by this mechanism.

2.3. Biotic Mechanisms for ROS Production in the Subsurface

In the subsurface, where photosynthesis does not occur because of the absence of sunlight, it is probable that some aerobic microbes can reduce O_2 to ROS (Yu and Kuzyakov, 2021). Heterotrophic bacteria can secrete extracellular nicotinamide adenine dinucleotide (NADH) or nicotinamide adenine dinucleotide phosphate (NADPH) oxidizing enzymes, which transfer electrons from NADH or NADPH to O_2 resulting in $^{\bullet}O_2^-$ production (Diaz et al., 2013; Zhang et al., 2016b). Other ROS can be further formed from $^{\bullet}O_2^-$ transformation (Yu and Kuzyakov, 2021). Since $^{\bullet}O_2^-$ does not permeate through cell membrane, the contribution of intracellular $^{\bullet}O_2^-$ to extracellular $^{\bullet}O_2^-$ production is usually negligible (Hansel and Diaz, 2021; Plummer et al., 2019). Within cells or on their surface, $^{\bullet}O_2^-$ can be transformed to H_2O_2 in the presence of superoxide dismutase (SOD), and the resulting H_2O_2 can pass through cell membranes (Bond et al., 2020; Hansel and Diaz, 2021; Schneider et al., 2016; Zinser, 2018). Further, both catalase and peroxidase can mediate the degradation of H_2O_2 (Sutherland et al., 2020), however the mechanism by which microbes produce •OH using $^{\bullet}O_2^-$ or H_2O_2 as precursors through nonphotochemical pathways is poorly understood and requires further investigation. As ROS production by biotic mechanism depends on the presence of O_2 and aerobic heterotrophic bacteria (Yu and Kuzyakov, 2021), it only contributes to ROS distribution in the oxic shallow subsurface, and cannot produce ROS in the anoxic deep subsurface which lacks sufficient aerobic heterotrophic bacteria. It is notable that biotic mechanisms can produce $^{\bullet}O_2^-$ and H_2O_2, but cannot

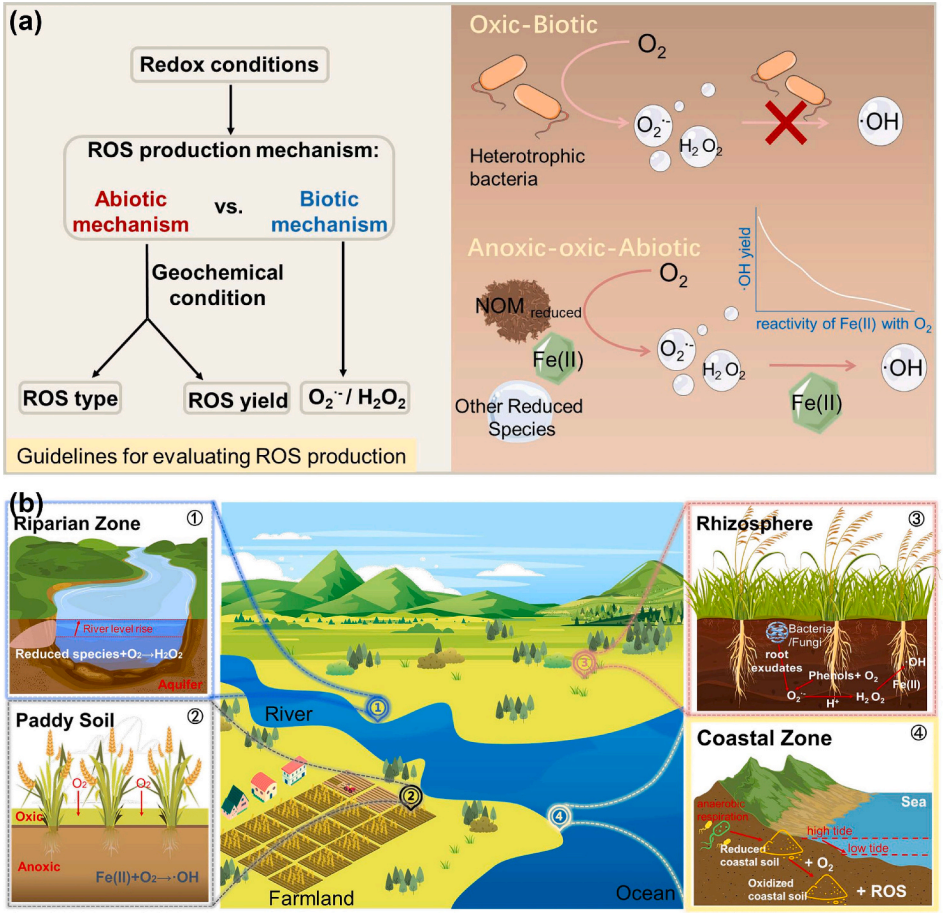

Fig. 2. Controlling mechanisms and typical scenarios for ROS production in the subsurface. (a) Guidelines for evaluating ROS production. In the subsurface, the types, production efficiency, and production mechanism of ROS are influenced by the redox conditions and by the geochemical conditions. The biotic mechanism mainly plays a role under oxic conditions, while the abiotic mechanisms predominate when reductive conditions are disturbed by O_2. (b) Typical scenarios of ROS production. These scenarios include the riparian zone, paddy soils, rhizosphere and coastal zone. In these scenarios, artificial activities and natural processes create favorable conditions for the coexistence of O_2 and reduced components, thereby contributing to ROS production.

produce •OH (Diaz et al., 2013; Sekar and DiChristina, 2014; Yu and Kuzyakov, 2021). Without photosynthesis, ROS production from biological H_2O oxidation is presumably impossible in the subsurface.

2.4. Theoretical and Empirical guidelines for evaluating ROS Production in the Subsurface

The above discussion suggests that both abiotic and biotic mechanisms can contribute to ROS production in the subsurface. Since the abiotic mechanism due to H_2O oxidation is of minor importance, as evidenced by the observation of negligible ROS production under anoxic conditions (Chen et al., 2021a; Tong et al., 2016), here we only discuss the theoretical and empirical rules controlling the importance of abiotic and biotic mechanisms of ROS production by O_2 reduction. The two mechanisms may predominate under different redox and geochemical conditions (Fig. 2a). The first theoretical criterium to distinguish abiotic and biotic mechanisms is the redox condition (Fig. 2a). Abiotic mechanisms predominate when reducing conditions are disturbed by O_2 (Tong et al., 2016). This scenario may result in reduction of O_2 to ROS by reduced components in the subsurface. As aerobic heterotrophic bacteria are either absent or cannot grow to a sufficient biomass in a short time, biotic mechanisms are not expected to contribute significantly (Chen et al., 2021a; Tong et al., 2016). When the redox conditions change from reductive to oxidative with complete oxidation of reduced components, and aerobic heterotrophic bacteria grow successfully, the predominant mechanism may evolve from abiotic to biotic accordingly (Fig. 2a). That is to say, biotic mechanisms predominate under oxic conditions in the presence of aerobic heterotrophic bacteria.

For the abiotic mechanism, a further criterium on which to evaluate the likelihood of ROS production is the geochemical composition of the solid and aqueous matrices (Fig. 2a). As the solid matrix in the subsurface has a much greater abundance of reduced species than the aqueous phase (Barcelona and Holm, 1991), the composition of the solid matrix plays a more important role (Tong et al., 2016). In particular, the abundance and speciation of Fe(II), NOM and S(-II) in the solid phase determines the rate and extent of O_2 activation and the resultant ROS production (Chen et al., 2021a; Du et al., 2021). The electron utilization efficiency of different Fe(II) species for •OH production approximately follows the order: ligand complexed Fe(II) > Fe(II) in phyllosilicate > surface adsorbed Fe(II) > iron sulfide mineral and siderite > dissolved Fe^{2+} (Table 1). Although the NOM and complexed Fe(III) in the aqueous phase do not contribute to any significant extent, they may act as shuttles to facilitate ROS production and to expand the area of ROS distribution (Wei et al., 2024; Yu et al., 2021a). The electron utilization efficiency of Fe(II) in soils and sediments for •OH production is 0.9–3.0 %, while the electron utilization efficiencies of dissolved NOM and ligand-complexed Fe(II) can be as high as 10.5–36 % and < 5.1–42.3 %, respectively (Table 1). When electrons are transferred from solid Fe(II) in soils and sediments to dissolved NOM and ligand complexed Fe(III), the resulting reduced NOM and ligand complexed Fe(II) significantly enhance •OH production. For example, the addition of ligands such as EDTA and TPP have been shown to elevate the electron utilization efficiency of Fe(II) in sediment from 1.7 % to 3.2–14.1 % (Table 1). When there is insufficient O_2 concentration present to oxidize all the reduced species in the aqueous phase, the surplus reduced species can be transported by the groundwater flow to a larger area (Wei et al., 2024). This transport expands the area for ROS production and distribution.

Besides the above two theoretical guidelines, we further propose the following empirical guidelines. The first is the duration and frequency of O_2 perturbation of the reductive conditions. A long duration of O_2 perturbation may completely change the redox condition from reductive to oxidative. Thus, an ideal case involves frequent O_2 perturbation of the reductive conditions, allowing the coexistence of O_2 and reduced species over a certain time and space window (Zhang et al., 2020a). For a certain duration of O_2 perturbation, the gradual oxygenation of reduced species in the subsurface produces ROS; when O_2 perturbation is terminated, the reduced species can be regenerated by intrinsic biogeochemical processes with the result that ROS production recommences on onset of the next O_2 perturbation event (Hu et al., 2023; Huang et al., 2023). This process may become cyclic with the cycle period dependent on the frequency of O_2 perturbation events. As illustrated in Fig. 2b, typical scenarios of ROS production include riparian zones influenced by seasonal water level fluctuations, paddy soils influenced by regular flooding and drainage, root rhizosphere influenced by daily O_2 secretion, coastal zones influenced by tide.

The second empirical guideline is the texture of subsurface matrixes. As reduced species are normally enriched in the low-permeability matrices (Aeppli et al., 2022), i.e., silty and clayed layers, we deduce that the areas around the low-permeability matrices are hotspots for abiotic ROS production. ROS production is constrained to the near proximity of reactants in a low-permeability matrix or the interface between low- and high-permeability matrices because the slow water flow in low-permeability matrices does not allow for the deep penetration of dissolved O_2. For sandy matrices which contain low contents of reduced species, ROS production is not intensive (Xie et al., 2020). Heterogeneous matrices could be favorable for ROS production in the subsurface. A typical scenario is a sandy matrix with scattered low-permeability lenses or intercalated low-permeability layers. In this situation, a sandy matrix allows O_2 penetration, and a low-permeability matrix provides reduced species for O_2 activation.

2.5. Typical scenarios for ROS Production in the Subsurface

Production of ROS in the subsurface requires the interaction of reduced species and O_2 (Tong et al., 2016). As the coexistence of reduced species and O_2 is thermodynamically unfavorable, ROS production is kinetically limited to certain time or space windows (Yuan et al., 2017; Zhang et al., 2020a). Thus, ROS production in the subsurface occurs under redox-dynamic conditions, which render the coexistence of reduced species and O_2 possible in a certain time window or in a specific space. The impact of ROS in transformation of redox-sensitive substance is also constrained to the hotspots in the subsurface under redox-dynamic conditions. Typical hotspots are located at the interfaces of oxic-anoxic zones or in the alternating oxic and anoxic environments, such as riparian and coastal zones, plant rhizospheres, paddy soils, etc. (Fig. 2b).

2.5.1. Riparian and Coastal zones Experiencing Water Table Fluctuations

Riparian and coastal zones are characterized by frequent water table fluctuations (Liu et al., 2024a; Zhao et al., 2022). These fluctuations can disturb the thermodynamically steady distribution of redox-active species, leading to the formation of a thermodynamically unstable zone with coexisting O_2 and reduced species favoring ROS production, as evidenced by the in situ detection of H_2O_2 in aquifers (Yuan et al., 2017; Zhang et al., 2020a). For instance, the steady-state concentration of H_2O_2 reached 123 nM in an unconfined aquifer near the Yangtze River (Zhang et al., 2020a) while H_2O_2 concentrations of up to 54 nM have been observed at the Rifle site in Colorado (Yuan et al., 2017). As O_2 and reduced species are prerequisites for ROS production, water table fluctuations, which govern the flux of O_2 and dissolved reduced species, regulate ROS accumulation and distribution. For instance, a rising water table in a riparian zone typically results in an increase in H_2O_2 production, whereas a falling or stable water table corresponded to low H_2O_2 concentrations (Zhang et al., 2020a). Besides the influence on dissolved component distribution, water table fluctuations also affect the reactivity of Fe-bearing minerals. A recent study noted that water table fluctuations induced the transformation of crystalline Fe minerals to redox-active metastable iron phases, enhancing surface Fe reactivity and ROS production (Zhao et al., 2022).

In addition to riparian aquifers, riparian soils have also recently been identified as hotspots for ROS production (Liu et al., 2024a), with the highest steady-state concentration of H_2O_2 reaching 539.7 μmol/kg

during oxygenation for 24 h. However, as riparian soils are typically above the groundwater tables, fluctuations in the groundwater table are not the primary driver for ROS production. Instead, meteorological conditions, such as temperature, precipitation and humidity, play crucial roles because they can influence microbial structure and biogeochemical rates as well as soil physicochemical properties (Liu et al., 2024a), thereby affecting ROS production from biotic and abiotic pathways.

2.5.2. Rhizosphere

The plant rhizosphere, the narrow zone of soil at the root–soil interface, is a highly redox-dynamic hotspot for intense biogeochemical processes (Philippot et al., 2013; Wei et al., 2019). Many plants (e.g., rice) transfer O_2 to the roots through aerenchyma, a process known as radial oxygen loss (ROL) into the rhizosphere (Philippot et al., 2013; Wang et al., 2018). ROL forms a narrow oxic or microoxic zone around the root leading to a gradually decreasing redox potential from the root surface to the bulk soil (Khan et al., 2016). The circadian rhythms of ROL in the rhizosphere under light-dark cycles make it advantageous to abiotic formation of ROS (Dai et al., 2022). Besides, abundant redox-active substances, such as phenols, quinones and iron minerals exist in the rhizosphere (Dias et al., 2016; Kaplan et al., 2016). The reactions of these substances with O_2 also provide favorable conditions for production of ROS. In addition to abiotic factors, biotic factors such as microbial communities also play an important role in ROS production in the rhizosphere through fueling the reduced species for O_2 activation (Liu et al., 2022). For example, Fe(III)-reducing microbes can reduce Fe(III) to Fe(II), thereby contributing to ROS production (Liu et al., 2022). The steady-state concentrations of $^{\bullet}O_2^-$ and H_2O_2 in sediment pore water in *Spartina alterniflora*-dominated salt marsh systems can reach nM and nM–μM levels, respectively (Dias et al., 2016), comparable to those in surface water (Petasne and Zika, 1987; Shaked et al., 2010). The discovery of ROS in the rhizosphere provides new sights into the biogeochemical processes in this important niche.

2.5.3. Paddy Soils

Paddy soils are regarded as the "grain base" for food production, providing food for 50 % of the world population (Kögel-Knabner et al., 2010). The cultivation of rice in these soils involves regular flooding and drainage, which triggers the reductive dissolution of Fe(III) minerals and the reoxidation of Fe(II) species. This process results in a significant and sustained production of ROS (Chen et al., 2021a; Huang et al., 2023). In addition to the flooding and drainage, O_2 secretion by rice roots can create an anoxic-oxic dynamic microenvironment, leading to ROS production from oxidation of rhizosphere Fe(II) by O_2 with these ROS contributing to the degradation of rhizosphere pollutants (Meng et al., 2023). The $^{\bullet}OH$ production capacity of paddy soils is estimated to be several hundred micromoles per kilogram (Chen et al., 2021a; Huang et al., 2023). Further, a recent study reported that H_2O_2 concentrations in paddy overlying waters, measured in an in situ experiment system, can reach 0.03–16.9 μM under nonphotochemical conditions (Liu et al., 2024b), which is significantly higher than those in the riparian zone (~ 123 nM) (Zhang et al., 2020a). This discrepancy may be attributed to the abundant reduced components and rapid supply of O_2 at the paddy soil-water interface (Liu et al., 2024b). These findings underscore the substantial potential of paddy soil systems for ROS production.

2.5.4. Other scenarios

Other scenarios for ROS production are increasingly being discovered, including groundwater abstraction and discharging (Zhang et al., 2023b), groundwater table fluctuations (Jia et al., 2017; Wei et al., 2024), sludge composting (Xing et al., 2022), remediation of contaminated groundwater through oxygenation (Cai et al., 2022), and oil/gas recovery with oxygen-containing water injection (Zhang and Jun, 2018). In these scenarios, the mechanisms of ROS production are mainly attributed to abiotic O_2 reduction by reduced components (such as Fe (II)). For instance, when groundwater is exposed to air during abstraction and discharging, notable amounts of H_2O_2 and $^{\bullet}OH$ are produced from the abiotic O_2 reduction by dissolved reduced components (Zhang et al., 2023b).

Table 2
Typical methods applied in the subsurface ROS detections.

ROS detection Methods	Application scenario	ROS species selectivity	Detection limit	Notes
EPR	Qualitative analysis, Lab-based & not suitable for field analysis	Medium–high	nM–μM	Multiple anti-facts exist in the spectrum
Spectroscopic probes	Quantitative analysis, Lab-based & partially suitable for field analysis	High	pM–nM	Subsurface matrixes interfere with the analysis
Spatial mapping	ROS distribution, Suitable for field analysis	Low	μM	Typically combined with other methods

3. ROS Measurement in the Subsurface

3.1. Challenges in Subsurface ROS Analysis

Quantifying and characterizing ROS in the subsurface is an endeavor fraught with great challenges due to the short lifetimes and low concentrations of ROS as well as the difficulties in preserving the redox condition of samples in a state similar to that in the natural environment (Burns et al., 2012). For instance, $^{\bullet}OH$ has a lifespan of nanoseconds to milliseconds, and $^{\bullet}O_2^-$ has a half-life ranging from seconds to minutes, contingent on its existing conditions (Daiber et al., 2004; Diaz et al., 2013; Hodges, 2003). Water samples from porous or fissure matrixes in the subsurface are difficult to collect, and the in situ redox conditions are prone to rapid to variation. These minuscule timeframes and complicated existing conditions make capturing and quantifying ROS a formidable task, demanding sophisticated analytical techniques and instrumentation.

Compounding the complexity of ROS measurements is the fact that natural subsurface environments are replete with intricate matrices, such as Fe(II) and natural organic matter (NOM). These components can introduce unwanted interferences, complicating the accurate assessment of ROS concentrations (Zhang et al., 2020a). The chemical interactions and reactivity of ROS with these substances further accentuate the challenge, making it imperative to employ meticulous experimental designs and analytical methodologies to ensure accurate and reliable measurements. Moreover, subsurface settings, whether in soil, sediment, or groundwater systems, are inherently heterogeneous. Variations in geology, chemistry, and microbial activity can lead to substantial spatial and temporal disparities in the distribution of ROS (Yuan et al., 2017; Zhang et al., 2020a). These disparities are not only scientifically intriguing but also hold practical significance for understanding and managing environmental processes. However, the acquisition of knowledge regarding the spatial and temporal dynamics of ROS in subsurface environments is highly challenging and require development of ROS detection methods with precise and appropriate spatio-temporal resolution.

3.2. ROS Identification and Quantification

Presently, the identification and quantification of ROS in the subsurface apply the chemical methods normally used from aquatic environments, and make modifications needed depending on the

characteristics of the experimental systems.

3.2.1. Electron Spin Resonance Analysis

Electron Spin Resonance (ESR) is a crucial analytical technique utilized for the detection of free radicals (Grün, 1989; He et al., 2014) (Table 2). Given the inherently short lifetimes of most free radicals, ESR employs spin trapping agents to capture these radicals, forming more stable spin adducts or complexes that can be readily analyzed (Dikalov et al., 2018). ESR spin-trapping is widely acknowledged as the gold standard for confirming the generation of ROS due to its high selectivity based on the distinct ESR spectra of the spin-trapped radicals. Furthermore, it provides semi-quantitative information regarding the ROS concentration, facilitating the assessment of ROS production rates or scavenging capacities. Nevertheless, ESR measurement relies on lab-based instrumentations and is not conducive for on-site analysis of ROS, especially in subsurface environments. Notably, ESR analysis can be interfered by multiple artifacts, and the intricate matrices (e.g., NOM) in the subsurface can introduce additional complexity (Nosaka and Nosaka, 2017). It is also critical to recognize that trapping agents must be used with ESR and, as such, the measured radical concentration represents a cumulative value of the radical concentration and does not represent the steady state concentration. The trapping agent added negates the effect of any radical consumption pathways and, as such, prevents measurement of actual in situ steady state concentrations.

3.2.2. Spectroscopic Analysis

Spectroscopic analysis involves techniques such as UV/vis absorbance, chemiluminescence, and fluorescence spectroscopy (Burns et al., 2012) (Table 2). Here we list some representative spectroscopic methods for $^{\bullet}O_2^-$, H_2O_2, and $^{\bullet}OH$ analysis. $^{\bullet}O_2^-$ has a short lifespan and its direct analysis is challenging. To address this issue, scavengers like superoxide dismutases (SOD) and nitro blue tetrazolium (NBT) are used to trap $^{\bullet}O_2^-$ and form stable spin adducts (Flohé and Ötting, 1984; Kakkar et al., 1984; Kono, 1978; Nandi and Chatterjee, 1988). However, direct detection via UV spectrophotometry is limited by the short wavelengths and weak extinction coefficients of the ROS (Bielski et al., 1985). To overcome these limitations, chemiluminescence methods have been developed, with 2-methyl-6-(4-methoxyphenyl)-3,7- dihydroimidazo [l,2-a] pyrazin3(7H)-one (MCLA) emerging as a more selective probe (eq. 12) (Nishinaka et al., 1993; Prónai et al., 1992). MCLA-based chemiluminescence assays offer a high sensitivity and specificity for $^{\bullet}O_2^-$, and they have been successfully employed to measure its concentrations in seawater (Rose et al., 2008a). However, quantifying $^{\bullet}O_2^-$ in the subsurface remains challenging due to the complex matrices and the influence of redox chemistry and biological processes. A solution to this challenge involves indirectly quantifying $^{\bullet}O_2^-$ by measuring the concentration of hydrogen peroxide (H_2O_2) formed through the disproportionation reaction of $^{\bullet}O_2^-$.

$$\mathrm{MCLA} + \dot{O}_2^{-} \rightarrow \mathrm{CO_2} + \mathrm{CL\ of\ product\ at}\ \lambda = 465\ \mathrm{nm} \quad (12)$$

H_2O_2 is characterized by a high stability and relatively long half-life, making it amenable to measurement in various environmental settings. Fluorescence and chemiluminescence methods are typically used to determine H_2O_2 concentrations (Burns et al., 2012). These methods rely on fluorescent probes, such as scopoletin (Boveris et al., 1977), 2′,7′-dichlorodihydrofluorescein (H_2DCF) (Zhou et al., 1997), and Amplex Red (AR) (eq. 13) (Rhee et al., 2010), which respond to H_2O_2 by producing a change in fluorescence intensity. Chemiluminescence methods employing luminol and 10-methyl-9-(*p*-formylphenyl)-acridinium carboxylate trifluoromethanesulfonate (AE) have also been developed for H_2O_2 detection (King et al., 2007; Yuan and Shiller, 2004). While these methods offer high sensitivity, it is important to consider potential interference from background fluorescence, especially in subsurface environments. For instance, to address the interference of soil/sediment components on H_2O_2 measurements, some studies estimate H_2O_2 concentrations by applying a calibration factor to the blank values (Trusiak et al., 2018; Zhang et al., 2024a). In addition, it is also a feasible strategy to add a chemical masking agent to eliminate the interfering ions (Burns et al., 2012; Yuan et al., 2017).

AR + horseradish peroxidase/H_2O_2 → Resorufin (Ex/Em = 540/590 nm) (13).

$^{\bullet}OH$ has a much shorter lifespan compared to other ROS, making direct detection challenging. To indirectly measure $^{\bullet}OH$, specific probe compounds, including benzoic acid (BA), salicylic acid (SA), and terephthalic acid (TPA), can capture and quantify $^{\bullet}OH$ in a system (Su et al., 2019). These compounds selectively react with $^{\bullet}OH$ to produce stable hydroxylation products, which can be separated and detected by chromatography or mass spectrometry. In the presence of solid matrices, caution should be paid to the sorption loss of hydroxylated products, which may lead to the underestimation of $^{\bullet}OH$ production.

3.2.3. Spatial Mapping

The distribution of reactive oxygen species (ROS) in the subsurface environment exhibits high spatial heterogeneity. Firstly, the sources of ROS generation are highly spatially heterogeneous. For example, dynamic interfaces such as soil-water-air-oxygen interfaces often serve as hotspots for ROS generation, leading to significant concentration differences in the range of mm to m scale. Additionally, the limited diffusion distances of ROS result in non-homogeneous distributions in both sources and bulk phases (Table 2). For instance, the concentration of singlet oxygen decreases to 50 % within 80 nm from the source, and to 0.1 % within 250 nm (Latch and McNeill, 2006). Similarly, the spatial distribution of $^{\bullet}OH$ also exhibits high heterogeneity in the nm-μm scale. Therefore, identifying and mapping the spatial distribution of ROS is crucial for accurately predicting the processes and effects of ROS under spatial differences. Currently, the development of in situ imaging detection methods and devices for ROS is still in its early stages. The Chu's research group has developed a technique combining in situ imaging gel films with fluorescence confocal microscopy, which enables in situ detection of environmental ROS at the μm-mm scale, and has explored ROS generation mechanisms and mm-scale spatial distribution in coastal sediments under tidal influence (Zhao et al., 2022). Furthermore, by utilizing a microfluidic chip platform combined with in situ imaging of ROS, they achieved μm-scale in situ online imaging of ROS in the rice root zone, visualizing the ROS generation hotspots at the rice root-soil interface (Dai et al., 2022).

3.3. Guidelines for Choosing the Most Suitable ROS Characterization Method

The selection of the most appropriate ROS characterization method depends on the specific research goals and the unique characteristics of the subsurface environment. Generally, for qualitative characterization, confirming the generation of ROS can be accomplished using ESR spectroscopy. Additionally, the relative contribution of ROS to redox-sensitive substance transformation can be determined by comparing transformation rates or efficiencies before and after introducing various quenching agents. It is important to consider the numerous interfaces present in the subsurface environment, as interfacial reactions must be factored in when choosing quenching agents. For quantitative characterization, ROS with certain half-lives such as H_2O_2 can be directly measured through sampling and subsequent chemical analysis. Conversely, for the ROS such as $^{\bullet}OH$ which exhibit shorter half-lives, direct sampling and measurement are impractical. In such cases, probe methods are employed to determine the rate of generation of $^{\bullet}OH$ but cannot determine the steady state concentration because of the negation of loss pathways as a result of the presence of the probe compound. To identify the spatial distribution of ROS in the subsurface environment, techniques with spatial resolution such as fluorescence imaging can be harnessed to analyze the distribution of ROS within specific regions, providing valuable information for investigating ROS dynamics. For the

heterogeneous subsurface environment, the methods described above apply to the measurement of ROS in the aqueous phase and, potentially, a fraction in the solid phase. However, it is currently a challenge to measure the concentration of ROS sorbed to the surface of solid matrices.

4. Significance of ROS in the Subsurface

The significance of ROS in the subsurface involves two aspects. One is the direct reaction between ROS and the target substance, i.e., contaminant attenuation or organic matter decomposition. The other is the influence of ROS on microbial metabolism and, subsequently, on the biogeochemical processes for transport and transformation of the target substance. Since $^{\bullet}O_2^-$ and H_2O_2 are often regarded as precursors for the production of highly reactive $^{\bullet}OH$, the environmental effect of $^{\bullet}OH$ appears to be of greater significance.

4.1. Contaminant Attenuation

The attenuation of contaminants as a result of oxidation by $^{\bullet}OH$ is emerging as a novel pathway in alternating oxic-anoxic environments (Huang et al., 2021b), challenging the prevailing paradigm that microbial aerobic oxidation and biotic/abiotic reduction are the dominant mechanisms. The high reactivity of $^{\bullet}OH$ positions its oxidation as a rapid and effective process for attenuating contaminants. A notable example is the finding that the $^{\bullet}OH$ generated upon oxygenation of soils/sediments resulted in a significant reduction of TCE half-life from 60 years under anoxic conditions to 0.25 years under oxic conditions (Schaefer et al., 2018). Extensive research efforts have focused on contaminant oxidation by $^{\bullet}OH$ produced from the oxidation of Fe(II)-containing minerals and sediments by O_2. The target contaminants encompass a diverse range of organic compounds (e.g., trichloroethylene (Schaefer et al., 2018), polycyclic aromatic hydrocarbons (Chen et al., 2021b), phenol (Cheng et al., 2020), tetracycline (Tong et al., 2016), 1,4-dioxane (Zeng et al., 2017), petroleum compounds (Liu et al., 2024c), polystyrene microplastics (Chen et al., 2021c), antibiotics (Chen et al., 2023), coking wastewater (Zhou et al., 2019), as well as inorganic compounds (e.g., arsenic (Tong et al., 2016), CdS (Huang et al., 2021a), etc.) (Table S2).

However, as the oxidation by $^{\bullet}OH$ is nonselective, reduced species such as Fe(II) and NOM may competitively consume $^{\bullet}OH$, thereby diminishing the oxidation efficiency of contaminants (Zhang et al., 2023a). For instance, in oxic Fe(II)/soil/sediment systems, the utilization efficiency of $^{\bullet}OH$ for contaminant transformation varies from 1 to 46.9 % (Table S2), which is substantially lower than the desired 100 %. Therefore, reduced species play a dual role in generating and quenching $^{\bullet}OH$. The quenching efficiency of a reduced species can be estimated by eq. 14. Assuming a target contaminant concentration of 10 μM and a typical rate constant of 1×10^9 M^{-1} s^{-1} for its oxidation by $^{\bullet}OH$, the quenching efficiency exceeds ~99 % when $Fe(II)_{dis}$ ($k_{Fe(II),\,^{\bullet}OH} = 5 \times 10^8$ M^{-1} s^{-1} (Rose and Waite, 2002)) concentration surpasses 2 mM. This dual functionality may explain the relatively sluggish natural attenuation of contaminants observed in environmental settings.

$$QE = \frac{\sum c_i k_{i,\cdot OH}}{\sum c_i k_{i,\cdot OH} + c_{contaminant} k_{contaminant,\cdot OH}} \times 100\% \quad (14)$$

where QE denotes the quenching efficiency; c_i and $c_{contaminant}$ signify the concentrations of co-existing reduced components and contaminants, respectively; $k_{i,\,^{\bullet}OH}$ and $k_{contaminant,\,^{\bullet}OH}$ represent the rate constants for the reaction of $^{\bullet}OH$ with co-existing reduced components and contaminants, respectively.

In addition to $^{\bullet}OH$, other ROS including H_2O_2 can also contribute to contaminant degradation. For example, the enhanced bisphenol A degradation by reaction with H_2O_2 in soils has been reported recently (Yu et al., 2025). Additionally, H_2O_2 is capable of reducing Mn from high to low oxidation state and extracellular $^{\bullet}O_2^-$ is involved in Mn(II) oxidation (He et al., 2025; Qi et al., 2024; Zhang et al., 2021). $^{\bullet}O_2^-$ and its disproportionation product H_2O_2 are also recognized to be capable of dissolving iron oxides by reduction of Fe(III) to Fe(II) (Fujii et al., 2006) but most interest in these ROS has arisen as a result of their role in the generation of $^{\bullet}OH$ and/or high valent metal species via Fenton or Fenton-like reactions (Miller et al., 2018; Trusiak et al., 2018; Yuan et al., 2022; Zhao et al., 2022).

4.2. Organic matter decomposition

The subsurface environments contain abundant NOM, representing a huge carbon (C) pool in the terrestrial ecosystem (Hicks Pries et al., 2017). Although most of the NOM in subsurface environments is mineralized by microbes and respired into the atmosphere over short timescales, recent studies have revealed that abiotic oxidation of NOM by $^{\bullet}OH$ contributes significantly to CO_2 emission or C storage in redox-dynamic subsurface environments (e.g., paddy soils (Chen et al., 2021a)). For example, organic matter has been shown to undergo abiotic oxidation by ROS through a series of reaction steps (Chen et al., 2020; Hu et al., 2023; Wang et al., 2017c). In detail, the DOM is initially attacked by $^{\bullet}OH$ through both hydroxylation and hydrogen abstraction pathways (Chen et al., 2021a; Hu et al., 2023; Zeng et al., 2020). The resulting hydroxylated aromatic radical can subsequently undergo structural rearrangement or react with O_2 to form quinones or open-chain carboxylic acids. This oxidative transformation results in a decrease in molecular weight and an increase in bioavailability (Hu et al., 2023; Zeng et al., 2020). Laboratory simulation experiments show that the relative contribution of $^{\bullet}OH$ oxidation to CO_2 production was 15.1–30.8 % for oxygenation of paddy soils (Chen et al., 2021a), 14.6–27.6 % for acidic sulfate-rich soils (Zhang et al., 2020b) and 17.5–26.4 % for riparian sediments (Liu et al., 2024a). However, the role of ROS for C cycling in the subsurface at the field scale has received much less attention so far. Therefore, the relative contributions of abiotic and biotically catalyzed reactions on NOM decomposition remain unclear, particularly for ecosystems with a large ROS production flux, e.g., paddy soils and riparian zones.

4.3. Influence on Biogeochemical Processes

Subsurface microbes are of paramount importance in a multitude of biogeochemical activities, encompassing nutrient cycling and the conversion of both organic and inorganic compounds (Ehrlich and Newman, 2008). The biogeochemical dynamics of certain elements and substances may indirectly intertwine with microbially driven alterations of NOM and mineral phases, especially (oxyhydr)oxide minerals of iron and manganese, iron-rich clays, and iron sulfides (Dong et al., 2023; Kappler et al., 2021). Given that ROS can induce DNA disruption, protein and amino acid oxidation, lipid peroxidation of membrane fatty acids, and biomolecular damage and cell demise (Taverne et al., 2018), it stands to reason that ROS possess the potential to incapacitate functional microorganisms involved in element cycling (Wang et al., 2017b), thereby exerting a profound influence on biogeochemical element and substance cycling (Dong et al., 2023). Numerous studies have documented that ROS influence the growth and functionality of diverse microbes, such as Fe(III)-reducing bacteria (Chen et al., 2018), Mn(II)-oxidizing bacteria (Tong et al., 2022), ammonia-oxidizing Archaea (Tolar et al., 2016), and planktonic and macrophytic cyanobacteria (Rose et al., 2005; Swanner et al., 2015). These influences subsequently lead to inhibition of bacterially-mediated processes such as Fe(III) reduction (Chen et al., 2018), Mn(II) oxidation (Learman et al., 2011), ammonia oxidation (Tolar et al., 2016), and Archaean oxygen production (Swanner et al., 2015). In addition, the disparate responses of microbes to ROS can result in the reshaping of the microbial community in the subsurface, and subsequently affect the associated biogeochemical processes (Ma et al., 2019). Besides influencing microbial activity and community structure, ROS may also affect extracellular enzymes, thereby impacting the

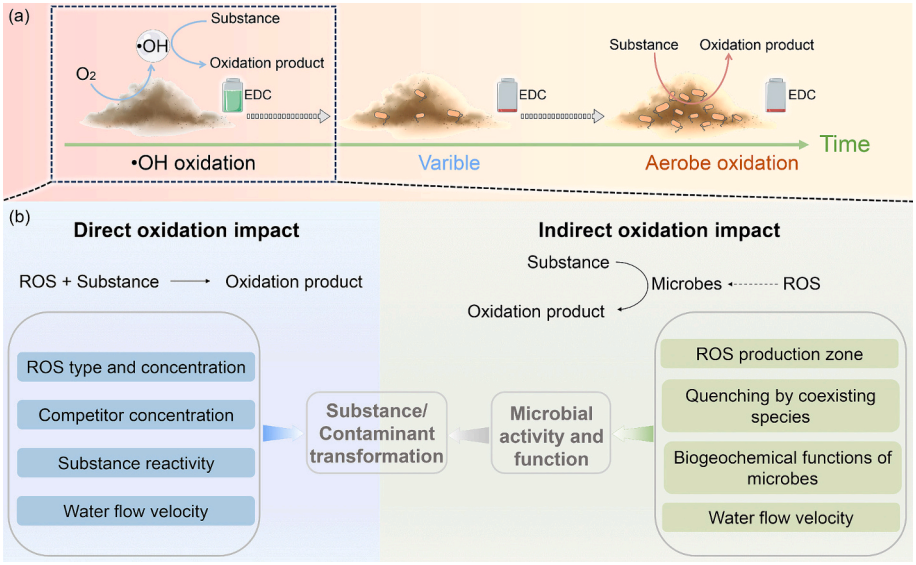

Fig. 3. Framework for assessing the importance of ROS oxidation on substance transformation in the subsurface. (a) Variation of substance oxidation mechanisms during oxygenation of reduced soils/sediments, where substance oxidation is initially dominated by •OH oxidation, followed by a stabilization period and finally by aerobic microbial oxidation. (b) Influence of environmental factors on the direct and indirect impacts of •OH.

biogeochemical cycling (Dong et al., 2023; Sheng et al., 2023).

4.4. Redox-Sensitive Substance Oxidation by ROS and Aerobic Microbes in the Subsurface

As discussed above, both aerobic biological oxidation and •OH-mediated oxidation contribute to redox-sensitive substance transformation in the subsurface (Ehrlich and Newman, 2008; Tong et al., 2016). Aerobic biological oxidation, which requires a high abundance of aerobic bacteria, typically occurs in oxic surface environments (Fig. 3a). In contrast, •OH oxidation, which occurs during the oxygenation of reduced species including Fe(II) and reduced NOM, is prevalent at oxic-anoxic interface (Fig. 3a). When the reduced species are consumed, the redox conditions of soils and sediments change from anoxic to oxic, thus stimulating the growth of aerobic and facultative bacteria and triggering aerobic biological oxidation (Fig. 3a). A recent study conducted by Li et al. (2024) reported a three-stage oxidation pattern of contaminants during oxygenation of sediments, with a first stage of •OH oxidation followed by a long stabilization stage and finally an aerobic biological oxidation stage. The stabilization stage temporally separates •OH oxidation from microbial oxidation, thereby diminishing the inhibitory effect of •OH on aerobic microbes and creating favorable conditions for the enrichment of aerobic microbes. The duration of the stabilization stage was shown to be highly dependent on the properties of soils and sediments (Li et al., 2024). Soils and sediments rich in aerobic and facultative microbes, particularly those capable of degrading the target substance and those with abundant nutritional conditions, typically experience a shorter stabilization stage.

4.5. Guidelines for evaluating the significance of ROS in the Subsurface

The guidelines for evaluating the significance of ROS in the subsurface can be summarized as follows (Fig. 3b). The direct impact of ROS in substance transformation is mainly controlled by the concentrations and types of ROS produced, the concentrations of background competitors for ROS, the reactivity of the redox-sensitive substance to ROS, and water flow velocity. First, the concentration of in situ generated •OH plays a dominant role as •OH is the most important ROS for direct substance transformation. •OH production can be evaluated by the theoretical and empirical guidelines mentioned above. Second, the background competitors for ROS determine the utilization fraction of •OH for the target substance transformation, which can be estimated by the equation for quenching efficiency (eq. 14). Third, the rate constants of substance (i.e., contaminants and organic matters) oxidation by •OH also have an important influence, which has been considered in the quenching efficiency. Finally, water flow determines the reaction time between ROS and target substance, and also transport the relatively long-lived ROS (particularly H_2O_2) from the production zone to some distance away for additional •OH production. The transport distance can be estimated by reactive transport modeling. The relative importance of ROS in substance transformation can be evaluated by kinetic modeling in soil/sediment systems or by reactive transport modeling in groundwater systems, as discussed later. For example, the addition of ligands can effectively promote •OH production during sediment oxygenation, thereby enhancing contaminant degradation (Xie et al., 2021). However, this enhancement is strongly influenced by both ligand type and concentration. Although •OH yield during sediment oxygenation is higher with the addition of EDTA than TPP, TCE degradation shows the opposite pattern (Xie et al., 2021). This has been attributed to the ability of EDTA, relative to TPP, to compete more strongly with TCE for the generated •OH. In addition, while higher concentrations of EDTA can lead to increased •OH production, the overall contaminant degradation efficiency decreases.

In contrast to the direct impact of ROS, the indirect impact arises from the stress induced by ROS on microbial activity and the subsequent reduction in ability of microbes to drive the biogeochemical transformation of substances present in the subsurface. As such, the relative importance of the indirect impact is mainly governed by the concentrations of ROS produced outside and inside of the microbial cells, the coexisting species scavenging ROS, the biogeochemical functions of microbes, and also water flow velocity. The concentrations of ROS produced outside and inside of microbial cells, particularly the latter, largely influence the metabolic activity and function of microbes. Both extra- and intracellular ROS can be scavenged by coexisting reduced species present in external environment and the enzymes that are capable of scavenging ROS inside the cells. The steady-state concentration of ROS, particularly inside cells, is the main determinant of the impact of ROS on microbial activity and function. It is difficult at present to estimate the relative importance of the indirect ROS-induced transformation of contaminants because the quantitative dose-effect relationship between ROS and the biogeochemical transformation of particular substances is not clear.

Table 3
A simplified reaction network for kinetic modeling of ROS production from a pulsed event of soil/sediment oxygenation.

No.	Reactions	Rate constant	References
	ROS production from Fe(II) oxidation		
1	$Fe(II) + O_2 \rightarrow Fe(III) + {}^{\bullet}O_2^-$	0.01–2.6 $M^{-1}\cdot s^{-1}$ [a]	(Zhang et al., 2023a)
2	$Fe(II) + {}^{\bullet}O_2^- \rightarrow Fe(III) + H_2O_2$	8×10^5 $M^{-1}\cdot s^{-1}$	(Chen et al., 2021a)
3	$Fe(II) + H_2O_2 \rightarrow Fe(III) + OH^- + \varphi_1{}^{\bullet}OH$ [b]	$3.9–5 \times 10^2$ $M^{-1}\cdot s^{-1}$ [a]	(Zhang et al., 2023a)
4	$Fe(II) + {}^{\bullet}OH \rightarrow Fe(III) + OH^-$	$1 \times 10^8–5 \times 10^8$ $M^{-1}\cdot s^{-1}$ [a]	(Zhang et al., 2023a)
5	$Fe(III) + O_2^- \rightarrow Fe(II) + O_2$	6.5×10^{-2} $M^{-1}\cdot s^{-1}$	(Rose and Waite, 2005)
6	$Fe(III) + H_2O_2 \rightarrow Fe(III) + O_2 + H_2O$	3.1×10^{-2} $M^{-1}\cdot s^{-1}$	(Kwan and Voelker, 2002)
	ROS production from NOM_{red} oxidation		
7	$H_2Q + O_2 \rightarrow Q + H_2O_2$	0.8 $M^{-1}\cdot s^{-1}$	(Yu et al., 2022)
8	$H_2Q + H_2O_2 \rightarrow {}^{\bullet}SQ + OH^- + \varphi_2{}^{\bullet}OH$ [b]	31 $M^{-1}\cdot s^{-1}$	(Yu et al., 2022)
9	$^{\bullet}SQ + H_2O_2 \rightarrow Q + OH^- + \varphi_2{}^{\bullet}OH$ [b]	4×10^2 $M^{-1}\cdot s^{-1}$	(Zhang et al., 2022b)
10	$H_2Q + Q \leftrightarrow 2{}^{\bullet}SQ$	$k_+ = 1 \times 10^7$ $M^{-1}\cdot s^{-1}$, $k_- = 2 \times 10^6$ $M^{-1}\cdot s^{-1}$	(Song and Buettner, 2010; Yu et al., 2022)
11	$NOM + {}^{\bullet}OH \rightarrow 0.18LMWOAs + 0.3CO_2 + 0.52X$ [c]	3.8×10^7 $M^{-c-1}\cdot s^{-1}$	(Yu et al., 2022)
12	$H_2Q + Fe(III) \rightarrow {}^{\bullet}SQ + Fe(II)$	2×10^3 $M^{-1}\cdot s^{-1}$	(Yuan et al., 2017)
13	$^{\bullet}SQ + Fe(III) \rightarrow Q + Fe(II)$	9×10^6 $M^{-1}\cdot s^{-1}$	(Yuan et al., 2017)
14	$^{\bullet}SQ + Fe(II) \rightarrow H_2Q + Fe(III)$	1×10^5 $M^{-1}\cdot s^{-1}$	(Yuan et al., 2017)

[a] The rate constants of k_1, k_3 and k_4 were set 0.1, 10 and 3×10^8 $M^{-1}\cdot s^{-1}$, respectively. Details are shown in Section S1.
[b] The value of φ_1 was reported to be 0–5.3 %. For the sake of simplification, the value of φ_1 was set at 4.1 %.
[c] X represents the partially oxidized NOM by •OH.

5. Quantifying the Rate and Flux of ROS Production and significance in the Subsurface

To evaluate the importance of ROS in the subsurface, it is necessary to quantify their rate of production. The redox-dynamic subsurface can be separated into two scenarios with these scenarios defined by the intensity of water flow. One scenario is the soil/sediment system with minimal water flow, and the other is the groundwater system with significant flow. For these two scenarios, different modeling tools are required to quantify the rate of ROS production and the resultant transport (or flux).

5.1. Rate of ROS Production in Soil/Sediment Systems

Given the challenge of measuring ROS in the field, monitoring the flux of ROS production in the shallow soil/sediment system is a difficult task. An ideal approach to estimate ROS in this system is solute reactive transport modeling in unsaturated zones, which is complicated by the multi-species (e.g., O_2 and Fe(II)) in the solid-gas-water multi-phase system. As an alternative simpler approach, we can approximately estimate the rate of ROS production through kinetic modeling by assuming soils/sediments as static systems. The conventional kinetic models, such as pseudo-first/s-order kinetic models, are simplistic for modeling soil/sediment systems. Instead, numerical kinetic models, based on a comprehensive reaction network encompassing ROS production and consumption, can be useful. The numerical kinetic models have been developed to describe ROS production from the oxidation of specific reduced species (i.e., Fe(II) and reduced NOM) by O_2 and H_2O_2 (Chen

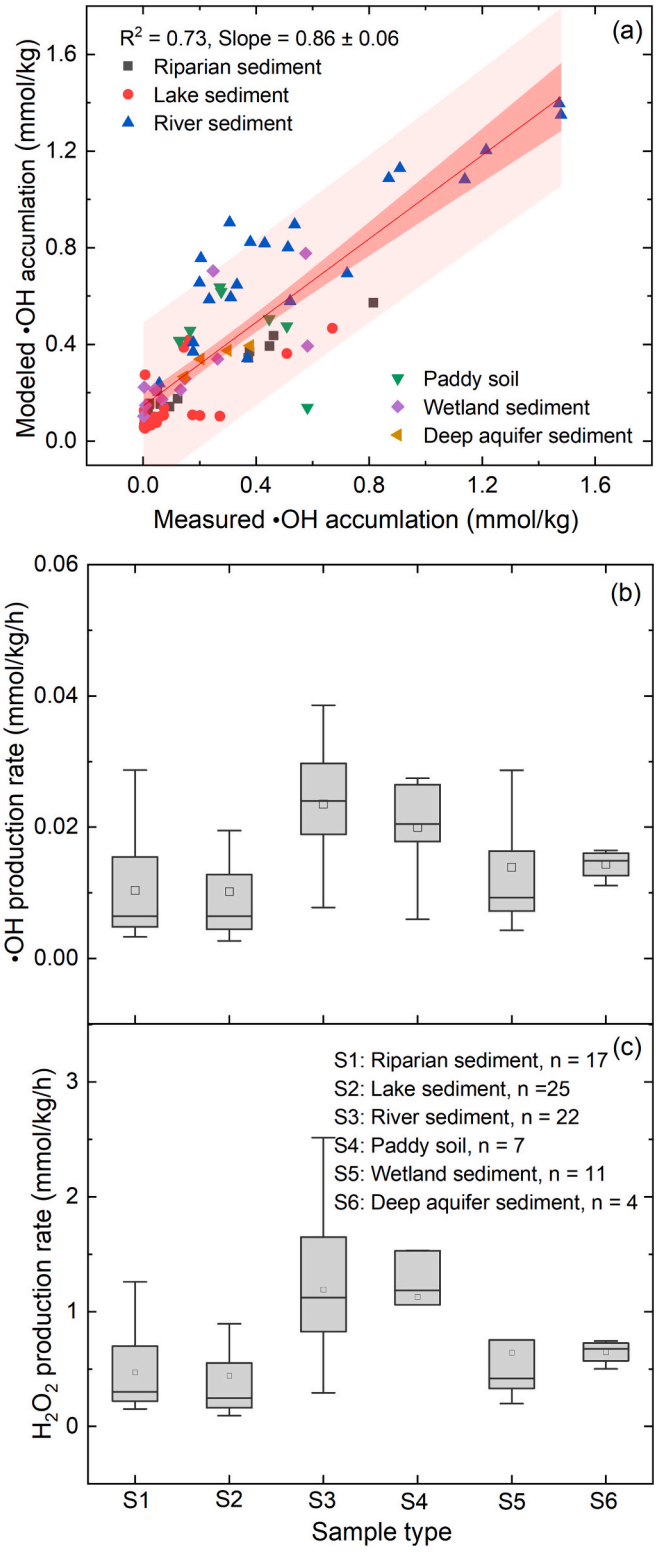

Fig. 4. ROS production rate. (a) Comparison between modeled and measured •OH. (b-c) modeled •OH and H_2O_2 production rates during oxygenation of soils/sediments. The calculations were derived from the reaction kinetic model outlined in Table 3. In panel a, the dark pink and light pink shades denote the confidence band and prediction band, respectively. (For interpretation of the references to colour in this figure legend, the reader is referred to the web version of this article.)

et al., 2023; Miller et al., 2016; Zhang et al., 2022b). However, simulating •OH production proves challenging due to the nonstoichiometric decomposition of H_2O_2 to •OH by Fe(II) and NOM (Remucal and Sedlak, 2011; Zhang et al., 2022b). For instance, the •OH production yield from H_2O_2 decomposition by inorganic dissolved Fe(II) is near 100 % at pH 3 but drops to ~0 % at pH 7 (Remucal and Sedlak, 2011); and the exact mechanism of •OH production from H_2O_2 decomposition by NOM remains unclear. The approaches addressing this issue involve the addition of side reactions that cannot produce •OH or can decompose •OH (Miller et al., 2013), the inclusion of more reactive intermediates like ferryl (Guo et al., 2021; Hug and Leupin, 2003), and the setting of experimentally measured •OH production yield (Zhang and Yuan, 2017; Zhang et al., 2022b). Consideration of side reactions or more reactive intermediates increases modeling complexity and uncertainty, as the mechanism of •OH production from H_2O_2 decomposition is not well understood (Remucal and Sedlak, 2011). Experimental measurement of •OH yield is simple but may deviate from the real case because reaction rates vary with the temporal variation of conditions like Fe(II) and NOM speciation.

Another challenge for modeling is the diversity of reduced species with different reactivity. For Fe(II) in soils/sediments, we can categorize all the Fe(II) species into ion exchangeable, surface-adsorbed and mineral structural Fe(II) based on sequential chemical extractions (Chen et al., 2021a). This approach can describe •OH production during the oxygenation of Fe(II) in soils and sediments (Zhang et al., 2023a). For NOM, it could be feasible to use electron-donating capacity (EDC) and electron-accepting capacity (EAC) as proxies for the reduced and oxidized groups in NOM, respectively (Yu et al., 2022). To estimate ROS flux in soil/sediment systems, we have developed a numerical kinetic model with a simplified set of reactions (Table 3, Section S1). The modeled •OH values were approximately consistent with the measured values in literature ($R^2 = 0.73$, Fig. 4). The average rates of •OH and H_2O_2 production within 24 h were estimated to be 0.003–0.049 and 0.09–2.52 mmol/(kg·h), respectively (Fig. 4). Notably, the rate of H_2O_2 production surpasses that of •OH by 1–2 orders of magnitude (Fig. 4), which is in line with the low transformation yield from H_2O_2 to •OH (Table 3). The lower oxidizing ability of H_2O_2 facilitates its relatively long persistence in soils and sediments, enabling it to transport and react with reduced species (e.g., Fe(II)-bearing clay minerals) to produce •OH (Dong et al., 2018; Wang et al., 2017a; Yu et al., 2025). However, it is important to note that soil/sediment oxygenation often occurs as pulsed events, with short periods of oxygenation followed by long periods of anoxia. Hence, the estimated •OH and H_2O_2 production rates represent these ROS production during a pulsed oxygenation event.

The environmental impact of ROS can be also estimated by the kinetic model described above. Given that the yield of CO_2 from the decomposition of NOM by •OH is ~0.3 mol of CO_2/mol of •OH (Goldstone et al., 2002), the rate of CO_2 production is estimated to be 4×10^{-5}–6.5×10^{-4} g CO_2/kg/h soils/sediments during a pulsed oxygenation event (24 h) (Section S2). For the 1-day oxygenation of a sediment with the thickness of 0.5 m and the density of 2.65×10^3 kg/m^3, the rate of CO_2 emission induced by •OH oxidation is further estimated to be 0.05–0.86 g CO_2/h/m^2 during a pulsed oxygenation event (24 h) (Section S2), which is comparable to that produced from soil respiration (Dorrepaal et al., 2009). While a model-based estimation approach provides a fundamental framework for ROS-driven organic matter transformation, its application to actual subsurface environments remains challenging. Therefore, combining modeling and experimental measurements to quantify how and to what extent ROS contributes to CO_2 production helps us to better understand ROS-driven carbon dynamics. Carbon isotope analysis has shown considerable potential in quantifying CO_2 production by •OH oxidation (Zheng et al., 2025).

5.2. Flux of ROS Production in Groundwater Systems

To quantify ROS flux in groundwater systems with flow, reactive transport modeling is a suitable approach. As previous studies in this regard are limited, we outlined the modeling procedure. The reactive transport model can be described by the classical advection-dispersion-reaction equation (eq. 15) (Carrera et al., 2022). However, three key challenges must be addressed when developing a reactive transport model for ROS production in groundwater systems: (1) accurately modeling ROS production from abiotic O_2 reduction, (2) incorporating other related intricate redox reactions occurring in the systems, and (3) determining the ROS-related reaction rate constants at the macroscale. These challenges are closely associated with the setting of r_i.

$$\frac{\partial \theta C_i}{\partial t} = -\nabla\cdot(\boldsymbol{q}C_i) - \nabla\cdot(\boldsymbol{D}\nabla C_i) - \theta r_i \tag{15}$$

where C_i is concentration of species i in groundwater, q is Darcy velocity vector, D is the dispersion tensor, the reaction rate r_i embeds all contributions of reactions associated with species i.

Unlike kinetic models, the increase in the complexity of chemical reactions in reactive transport models may lead to an exponential increase in computational demands. Hence, it is impractical to include all the related reactions of ROS production from abiotic O_2 reduction by different reduced species in the reactive transport models. As ROS production fundamentally involves electron transfer from reduced species to O_2, a viable simplification is to use EDC and EAC to represent the quantities of reactive reduced and oxidized species, respectively. Consequently, ROS production from abiotic O_2 reduction can be expressed as eqs. 16–19. Considering the notable differences in physicochemical properties of dissolved and solid species, EDC and EAC should be divided into two phases (For details, see Table S1).

$$\mathrm{EDC} + \mathrm{O_2} \rightarrow \mathrm{EAC} + \dot{\mathrm{O}}_2^- \tag{16}$$

$$\mathrm{EDC} + \dot{\mathrm{O}}_2^- + 2\mathrm{H^+} \rightarrow \mathrm{EAC} + \mathrm{H_2O_2} \tag{17}$$

$$\mathrm{EDC} + \mathrm{H_2O_2} + \mathrm{H^+} \rightarrow \mathrm{EAC} + \varphi\dot{\mathrm{O}}\mathrm{H} + \mathrm{H_2O} \tag{18}$$

$$\mathrm{EDC} + \dot{\mathrm{O}}\mathrm{H} \rightarrow \mathrm{EAC} + \mathrm{OH^-} \tag{19}$$

For the second challenge, besides the abiotic oxidation of reduced species by O_2, microbial aerobic respiration and the redox cycling of elements such as carbon, nitrogen, iron and sulfur may also occur (Boye et al., 2017; Buessecker et al., 2022; Gootman et al., 2020). These reactions (such as microbial Fe(III) reduction), either directly or indirectly, influence the spatiotemporal dynamics of ROS. The third challenge arises from the influence of scaling effects and the pronounced spatiotemporal heterogeneity of reactants, which often prevents reactive transport models from directly incorporating the parameters derived from lab experiments (Carrera et al., 2022). Instead, statistical methods are essential to integrate field data and laboratory results to establish these parameters. Furthermore, the timescales of elementary reactions related to ROS span from milliseconds to days (Hofmann et al., 2008; Prommer et al., 2019; Roelandt et al., 2010), while solute transport in groundwater systems typically spans from days to months (Li et al., 2017). This characteristic bestows upon the reactive transport model, which couples solute transport with kinetic reactions, a strong numerical stiffness (Geiger et al., 2012; Wu et al., 2012; Yeh et al., 2009). This stiffness largely amplifies the computational demands, rendering macroscale simulations nearly infeasible (Kinsela et al., 2016; Kräutle and Knabner, 2007). As ROS reactions are mostly irreversible, conventional methods such as local equilibrium assumption fail to remove the numerical stiffness (Crincoli et al., 2020; Wu et al., 2012). Temporal scale analytical techniques such as the computational singular perturbation (CSP) method provide a solution to simplify the reaction mechanisms in the model, thus eliminating stiffness (Lam, 1993; Lam and Goussis, 1994). In addition, due to scarcity of ROS data for groundwater systems, the verification and calibration of models often rely on the datasets of other related redox-active species (i.e., O_2, Fe(II)).

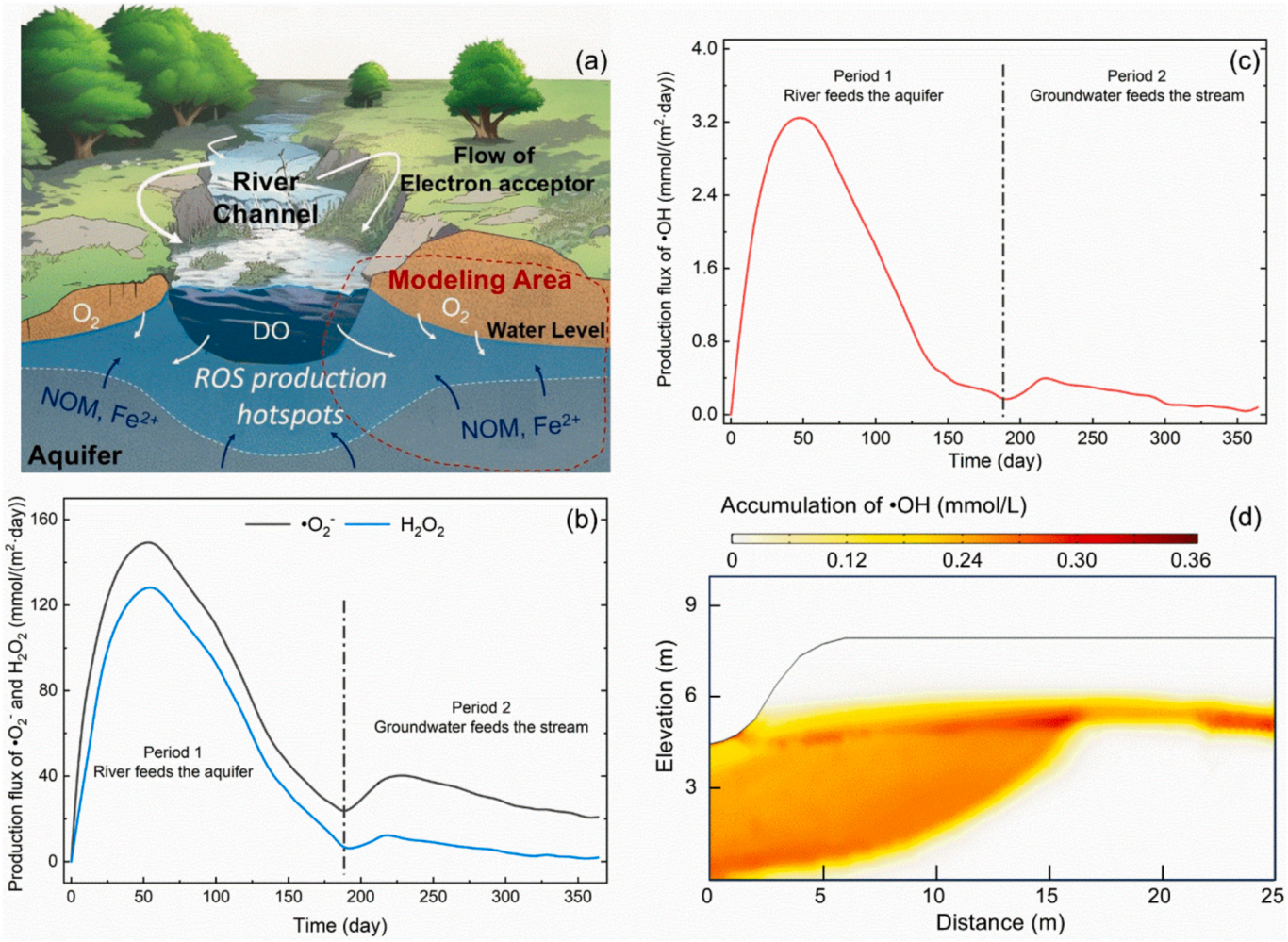

Fig. 5. (a) Scenario of ROS production in a riparian zone, (b, c) the production fluxes of $\bullet O_2^-$, H_2O_2 and •OH in the aquifer profile during one hydrological year and (d) the distribution of •OH accumulation within one hydrological year in the profile. Note that the flux of ROS means the integration of ROS production with the modeling area divided by the area of the river-aquifer interaction interface.

As O_2 in groundwater systems is generally limited, the time and space windows for ROS production are heavily dependent on the transport of O_2 (Zhang et al., 2020a).

To estimate ROS production flux in groundwater systems, we assumed a small-size riparian aquifer (Fig. 5a) and developed an illustrative 2D reactive transport model to demonstrate the dynamics of $\bullet O_2^-$, H_2O_2 and •OH generation and decay in one hydrological year (Section S3). The flux ranges for $\bullet O_2^-$, H_2O_2 and •OH within a typical riparian aquifer profile are 20.28–153.22, 1.33–132.67 and 0.03–3.29 mmol/(m^2·day), respectively (Fig. 5b, c). The hotspot of •OH production is mainly distributed in the redox transition zones (Fig. 5d), which aligns with distribution pattern of H_2O_2 in riparian zones reported previously (Zhang et al., 2020a). Assuming a complete reaction of produced •OH with NOM, the estimated amount of CO_2 production ranges from 0.00026 to 0.0456 g CO_2/(m^2·day), which was much lower than the CO_2 yield during a pulsed oxygenation event (0.05–0.86 g CO_2/h/m^2). This discrepancy may be partially attributed to the differences in O_2 supply between the two scenarios.

The illustrative model developed in this study provides a foundational framework for estimating ROS production and its environmental effects. Our findings suggest that the potential environmental consequences of high ROS concentrations warrant considerable attention, highlighting the broader significance of reactive transport models in advancing research in this field. It is important to emphasize that this model serves primarily as a proof of concept, intending to illustrate the potential of reactive transport models in estimating ROS production flux.

6. Perspectives

From the ROS research status described above, we conclude that a general framework for understanding ROS behavior in the subsurface has been formed (Figs. 1–3), whereas an in-depth understanding of the production and impact of ROS still requires advancement of both methodologies and fundamental theory. To guide future studies in this rapidly evolving area, we propose the following six areas of particular research needs.

6.1. Fundamental Mechanisms of ROS Production

The primary mechanism of abiotic ROS production in the subsurface has been ascribed to the activation of O_2 by reduced species. Key open questions remain however regarding the fundamental mechanisms of ROS production with particularly important knowledge gaps in the following areas.

(1) What's the principles and mechanisms controlling the yields of $\bullet O_2^-$, H_2O_2 and •OH from O_2 reduction by different types of reduced species. The molecular scale reactions of O_2 and the reaction of its intermediates ($\bullet O_2^-$ and H_2O_2) with reduced species

should be resolved so that quantum chemical calculations and well-controlled experiments can be performed to gain further insight into these mechanisms. It is also unknown why some reduced species can reduce O_2 sequentially to •OH but others cannot. For instance, the reduction of O_2 by ion exchange Fe(II) does not result in the production of •OH, whereas complexed and mineral structural Fe(II) do produce •OH (Xie et al., 2020).

(2) How abiotic and biotic mechanisms co-contribute to the production of different ROS, and how the interplay between abiotic and biotic mechanisms can be quantified. It has been established that abiotic and biotic mechanisms predominantly contribute to ROS production under anoxic-oxic dynamic conditions and oxic conditions, respectively (Chen et al., 2021a; Tong et al., 2016; Zhang et al., 2024a). When redox conditions change, both abiotic and biotic mechanisms may co-contribute to ROS production. However, the interplay between abiotic and biotic mechanisms, and how these potentially intercoupled processes proceed, remain unclear.

(3) Whether and how the electrons in separate subsurface zones can be transferred to O_2 for ROS production. In the subsurface, most reduced species exist in the form of particles, aggregates, and low-permeability lenses, interlayers or aquitards. However, the outer layer of these solid forms can interact with O_2, and the dominant inner space is physically separated from O_2 present in the flowing groundwater. As such, the question of whether and to what extent the reduced species in the inner space can donate electrons to O_2 in the porewaters requires resolution.

6.2. ROS Detection Method

After nearly half a century of development, environmental analysis techniques for ROS have reached the point of meeting basic qualitative and quantitative analysis needs. However, advances in time- and space-resolved detection, which are critically needed for ROS detection in subsurface environments, have been limited. This is attributed to the difficulty in capturing transient processes of ultrashort-lived ROS in the subsurface with current technologies (Yu et al., 2025). In addition, the high degree of soil/sediment heterogeneity makes microscale in situ ROS imaging difficult, and destructive sampling or macroscopic monitoring makes it hard to accurately identify the hotspots of ROS production in the subsurface (Wang et al., 2024; Yu et al., 2025). Therefore, it is essential that there be breakthroughs in time-resolved online analysis and spatially resolved in situ imaging technologies for ROS. This would allow us to clarify the dynamic evolution and effects of environmental ROS and to improve our understanding of significant subsurface processes mediated by ROS, such as nutrient transformation, pollutant fates, and even global elemental cycling. Future research on ROS analysis technology could focus on the following areas.

(1) High temporal-resolution ROS analysis technology and associated online recording. Currently, only the online monitoring of $•O_2^-$ and H_2O_2 has been achieved, and the range of ROS species that can be analyzed online needs to be expanded further. In terms of time resolution, the current seconds-level time resolution should be pushed further towards ultra-high time resolution in the range of microseconds to nanoseconds and even femtoseconds, laying the foundation for analyzing the dynamic evolution of environmental ROS. Ultra-high temporal resolution techniques in the range of fs-μs can also provide important evidence for elucidating ROS reaction processes and mechanisms.

(2) High spatial-resolution in situ imaging technology for ROS. At present, in situ imaging of ROS can only detect total ROS; there is an urgent need to develop highly selective in situ imaging technologies for a range of ROS. Additionally, the exploration of ultra-high spatial resolution in situ imaging technologies in the nm-μm scale for ROS and the development of nano-sensors to visualize and target ROS hotspots are required to provide methods for studying non-homogeneous ROS processes at important subsurface interfaces.

(3) Portable field analysis equipment for ROS. Currently, most environmental ROS research is based on laboratory simulations, with very little field research conducted. The main reason for this is the lack of field ROS analysis equipment. Therefore, there is an urgent need to develop portable field analysis equipment for ROS based on the development of laboratory methodologies to establish a foundation for field ROS research.

6.3. ROS Footprint Tracing Methods

One important method that needs to be developed is the capability to identify whether and to what extent ROS are involved in specific processes or scenarios. For example, the well-recognized Haber-Weiss mechanism suggests that O_2 is sequentially reduced to $•O_2^-$, H_2O_2, •OH and finally H_2O, implying a 100 % flux of ROS for O_2 reduction to H_2O in the subsurface. In reality, this mechanism has never been quantitatively evaluated because we do not have available methods to trace the stepwise production of ROS. Besides, many previous studies claimed that •OH production could largely contribute to CO_2 emission and contaminant transformation in the subsurface but we do not have methods to directly quantify the involvement of •OH. It is critical that quantitative methods be developed to trace the footprints of ROS production and consumption in the environment. Isotope labeling and fractionation (i.e., triple O and ROS-target elements) could be a potential method to trace the involvement of ROS. O-isotope labelling could be a potential method to trace the source and fate of ROS in well-controlled experimental system. The premise of using isotope methods is that the specific isotope (i.e., O) can be preserved in the target substance (e.g., an O-containing organic) and does not exchange with background substances (particularly H_2O). Another challenge is the high-precision measurement of O isotope in a specific low-concentration substance such as an organic micropollutant.

6.4. Models for quantifying ROS contribution to substance transformation

In addition to the above tracing method, we also need models to quantitatively estimate the contribution of ROS to the transformation and production of a specific substance in the subsurface. There are two types of models which could fulfill this need. One is the kinetic model for static systems, and the other is reactive transport models for flowing systems.

(1) For kinetic modeling of static systems, efforts are required to clarify the elementary reactions involved and to specify the associated reaction rate constants so that the reaction set can be established. This could be difficult for •OH production because the associated mechanism is not fully understood. Kinetic models are presently constrained to specific reaction systems, and general models which are applicable to different systems are required.

(2) The challenges faced by reactive transport modeling of flowing systems are more complex and diverse. The goal of the ROS reactive transport model is to achieve assessment of ROS yield and its environmental effects at the field and larger scales, identify the conditions that favor ROS environmental function, and quantitatively describe the role of ROS in the substance-energy cycle of the subsurface environment. To achieve this goal, two main issues must be addressed. First, it is a considerable challenge to incorporate so many ROS-related reactions into the advection-diffusion equation. In particular, the time scales of the reaction terms range from seconds to days, greatly increasing computational costs or even make the calculation infeasible. Special effort is required to simplify the reaction terms without

significantly sacrificing model accuracy. Second, the ROS reaction network, as part of the molecular oxygen reduction process, is highly correlated and interacts with the redox biogeochemical processes of carbon, nitrogen, phosphorus, sulfur, and various redox-active metals. Therefore, ROS reactive transport simulation should focus on effective coupling with traditional biogeochemical models.

6.5. Utilization of ROS for Subsurface Remediation

One of the important goals of learning from nature is to serve nature through what have become known as, "Nature-based Solutions". From this perspective, ROS that are produced in the surface may be utilized for in situ surface remediation. For remediation purposes, there is a need to maximize the production of •OH in the subsurface and facilitate selective reaction with the target contaminants.

(1) To maximize •OH production, two main barriers must be resolved. The first hurdle is the supply of O2 into the subsurface because its saturation concentration in water is very low. It is not possible to supply large quantities of O2 at one time; instead, it is optimal to supply small quantities of O2 continuously or periodically during the remediation process. The second hurdle relates to the efficiency of •OH production from O2 reduction by the reduced species in the subsurface. Most of the reduced species likely to be present can reduce O2 to •O2− and H2O2, but only a small subset of these species can efficiently reduce H2O2 to •OH. As such, a large number of electrons in various reduced species can, potentially, be utilized for •OH production, but a large increase in the electron utilization efficiency is required. It is likely that a chemical which has a high electron utilization efficiency for •OH production and can collect and shuttle the electrons from various reduced species to the •OH production pathway will be required. In this regard, iron-binding ligands such as tripolyphosphate could be a good alternative as it can assist in maintaining Fe(III), a key electron shuttle, in solution (Xie et al., 2021).

(2) To maximize contaminant degradation, there is a need to improve the selectivity of •OH for the target contaminants. As •OH can react non-selectively with all the oxidizable species including the reduced species that induce O_2 reduction, the in situ generated •OH can be consumed by both the target contaminants and other oxidizable species. It is therefore of great importance to increase the reaction selectivity in the subsurface, particularly for contaminants that are present at concentrations lower than that of non-target oxidizable species. Future work could be directed to the construction of localized conditions which are favorable for the reaction between •OH and target contaminants. It is also important that the •OH production zone is close to the contaminant's location given the extremely short half-life of •OH. In this regard, further consideration should be given to alternate oxidants such as sulfate radicals and peroxymonocarbonate in view of their lower reactivity and longer half-life.

Currently, H_2O_2- and peroxydisulfate-based processes represent in situ chemical oxidation technologies utilizing ROS (Yu and Kuzyakov, 2021). However, the structural and redox heterogeneity of aquifers can lead to additional agent consumption and discourage the contact of ROS with contaminants (Aeppli et al., 2022; Wang et al., 2024). Enhancing remediation efficacy hinges upon increasing the activation efficiency, shortening transport distances, and prolonging reaction durations (Wang et al., 2023; Wang et al., 2024).

CRediT authorship contribution statement

S.Y. proposed the structure and core ideas of this work and P.Z. wrote the first draft. C. C. wrote the section of analysis methods and X. B. wrote the section about reactive transport model. Y. T. draw most of diagrams. M. T., H. W., H. D., D. Z. A. K., P. V. and D. W. reviewed and edited the paper. S. Y. funded the research.

Declaration of competing interest

The authors declare that they have no known competing financial interests or personal relationships that could have appeared to influence the work reported in this paper.

Acknowledgements

This work was supported by grants from the National Natural Science Foundation of China (No. 42025703) and National Key Technology Research and Development Program of China (2022YFC3701403).

Appendix A. Supplementary data

Supplementary data to this article can be found online at https://doi.org/10.1016/j.earscirev.2025.105230.

Data availability

Data will be made available on request.

References

Aeppli, M., Babey, T., Engel, M., Lacroix, E.M., Tolar, B.B., Fendorf, S., Bargar, J.R., Boye, K., 2022. Export of organic carbon from reduced fine-grained zones governs biogeochemical reactivity in a simulated aquifer. Environ. Sci. Technol. 56 (4), 2738–2746.

Aeschbacher, M., Vergari, D., Schwarzenbach, R.P., Sander, M., 2011. Electrochemical analysis of proton and electron transfer equilibria of the reducible moieties in humic acids. Environ. Sci. Technol. 45 (19), 8385–8394.

Andrews, S.S., Caron, S., Zafiriou, O.C., 2000. Photochemical oxygen consumption in marine waters: a major sink for colored dissolved organic matter? Limnol. Oceanogr. 45 (2), 267–277.

Ardo, S.G., Nelieu, S., Ona-Nguema, G., Delarue, G., Brest, J., Pironin, E., Morin, G., 2015. Oxidative degradation of nalidixic acid by nano-magnetite via Fe^{2+}/O_2-mediated reactions. Environ. Sci. Technol. 49 (7), 4506–4514.

Barcelona, M.J., Holm, T.R., 1991. Oxidation reduction capacities of aquifer solids. Environ. Sci. Technol. 25 (9), 1565–1572.

Bielski, B.H., Cabelli, D.E., Arudi, R.L., Ross, A.B., 1985. Reactivity of HO_2/O_2^- radicals in aqueous solution. J. Phys. Chem. Ref. Data Monogr. 14 (4), 1041–1100.

Bond, R.J., Hansel, C.M., Voelker, B.M., 2020. Heterotrophic bacteria exhibit a wide range of rates of extracellular production and decay of hydrogen peroxide. Front. Mar. Sci. 7, 72.

Borda, M.J., Elsetinow, A.R., Strongin, D.R., Schoonen, M.A., 2003. A mechanism for the production of hydroxyl radical at surface defect sites on pyrite. Geochim. Cosmochim. Acta 67 (5), 935–939.

Boveris, A., Martino, E., Stoppani, A., 1977. Evaluation of the horseradish peroxidase-scopoletin method for the measurement of hydrogen peroxide formation in biological systems. Anal. Biochem. 80 (1), 145–158.

Boye, K., Noël, V., Tfaily, M.M., Bone, S.E., Williams, K.H., Bargar, John R., Fendorf, S., 2017. Thermodynamically controlled preservation of organic carbon in floodplains. Nat. Geosci. 10 (6), 415–419.

Buessecker, S., Sarno, A.F., Reynolds, M.C., Chavan, R., Park, J., Fontánez Ortiz, M., Pérez-Castillo, A.G., Panduro Pisco, G., Urquiza-Muñoz, J.D., Reis, L.P., Ferreira-Ferreira, J., Furtunato Maia, J.M., Holbert, K.E., Penton, C.R., Hall, S.J., Gandhi, H., Boëchat, I.G., Gücker, B., Ostrom, N.E., Cadillo-Quiroz, H., 2022. Coupled abiotic-biotic cycling of nitrous oxide in tropical peatlands. Nat. Ecol. Evol. 6 (12), 1881–1890.

Burns, J.M., Cooper, W.J., Ferry, J.L., King, D.W., DiMento, B.P., McNeill, K., Miller, C.J., Miller, W.L., Peake, B.M., Rusak, S.A., Rose, A.L., Waite, T.D., 2012. Methods for reactive oxygen species (ROS) detection in aqueous environments. Aquat. Sci. 74 (4), 683–734.

Cai, Q., Zhang, Y., Zheng, Y., Liu, Y., Liu, Y., Yuan, S., 2022. Groundwater circulation enhanced electrobioremediation of 1,2-dichloroethane in a simulated heterogeneous aquifer. Environ. Eng. Sci. 39 (7), 606–615.

Carrera, J., Saaltink, M.W., Soler-Sagarra, J., Wang, J., Valhondo, C., 2022. Reactive transport: a review of basic concepts with emphasis on biochemical processes. Energies 15 (3), 925.

Chen, R., Liu, H., Tong, M., Zhao, L., Zhang, P., Liu, D., Yuan, S., 2018. Impact of Fe(II) oxidation in the presence of iron-reducing bacteria on subsequent Fe(III) bioreduction. Sci. Total Environ. 639, 1007–1014.

Chen, C., Hall, S.J., Coward, E., Thompson, A., 2020. Iron-mediated organic matter decomposition in humid soils can counteract protection. Nat. Commun. 11 (1), 2255.
Chen, N., Fu, Q., Wu, T., Cui, P., Fang, G., Liu, C., Chen, C., Liu, G., Wang, W., Wang, D., Wang, P., Zhou, D., 2021a. Active iron phases regulate the abiotic transformation of organic carbon during redox fluctuation cycles of paddy soil. Environ. Sci. Technol. 55 (20), 14281–14293.
Chen, N., Huang, D., Liu, G., Chu, L., Fang, G., Zhu, C., Zhou, D., Gao, J., 2021b. Active iron species driven hydroxyl radicals formation in oxygenation of different paddy soils: Implications to polycyclic aromatic hydrocarbons degradation. Water Res. 203, 117484.
Chen, S., Yang, Y., Jing, X., Zhang, L., Chen, J., Rensing, C., Luan, T., Zhou, S., 2021c. Enhanced aging of polystyrene microplastics in sediments under alternating anoxic-oxic conditions. Water Res. 207, 117782.
Chen, B.L., Xia, Y., He, R.X., Sang, H.Q., Zhang, W.C., Li, J., Chen, L.F., Wang, P., Guo, S. S., Yin, Y.G., Hu, L.G., Song, M.Y., Liang, Y., Wang, Y.W., Jiang, G.B., Zare, R.N., 2022a. Water-solid contact electrification causes hydrogen peroxide production from hydroxyl radical recombination in sprayed microdroplets. Proc. Natl. Acad. Sci. U. S. A. 119 (32), e2209056119.
Chen, N., Geng, M., Huang, D., Tan, M., Li, Z., Liu, G., Zhu, C., Fang, G., Zhou, D., 2022b. Hydroxyl radical formation during oxygen-mediated oxidation of ferrous iron on mineral surface: Dependence on mineral identity. J. Hazard. Mater. 434, 128861.
Chen, R., Liu, H., Zhang, N., Huang, Y., Deng, X., Jin, M., 2023. Flavins enhance the hydroxyl radical production from $FeCO_3$ oxygenation for organic pollutant degradation. Chem. Geol. 626, 121443.
Cheng, D., Yuan, S., Liao, P., Zhang, P., 2016. Oxidizing impact induced by mackinawite (FeS) nanoparticles at oxic conditions due to production of hydroxyl radicals. Environ. Sci. Technol. 50 (21), 11646–11653.
Cheng, D., Neumann, A., Yuan, S., Liao, W., Qian, A., 2020. Oxidative degradation of organic contaminants by FeS in the presence of O_2. Environ. Sci. Technol. 54 (7), 4091–4101.
Crincoli, K.R., Green, C., Huling, S.G., 2020. Sulfate radical scavenging by mineral surfaces in persulfate-driven oxidation systems: Reaction rate constants and implications. Environ. Sci. Technol. 54 (3), 1955–1962.
Dai, H., Wu, B., Chen, B., Ma, B., Chu, C., 2022. Diel fluctuation of extracellular reactive oxygen species production in the rhizosphere of rice. Environ. Sci. Technol. 56 (12), 9075–9082.
Daiber, A., Oelze, M., August, M., Wendt, M., Sydow, K., Wieboldt, H., Kleschyov, A.L., Munzel, T., 2004. Detection of superoxide and peroxynitrite in model systems and mitochondria by the luminol analogue L-012. Free Radic. Res. 38 (3), 259–269.
Dias, D.M.C., Copeland, J.M., Milliken, C.L., Shi, X., Ferry, J.L., Shaw, T.J., 2016. Production of reactive oxygen species in the rhizosphere of a Spartina-dominated salt marsh systems. Aquat. Geochem. 22, 573–591.
Diaz, J.M., Hansel, C.M., Voelker, B.M., Mendes, C.M., Andeer, P.F., Zhang, T., 2013. Widespread production of extracellular superoxide by heterotrophic bacteria. Science 340 (6137), 1223–1226.
Dikalov, S.I., Polienko, Y.F., Kirilyuk, I., 2018. Electron paramagnetic resonance measurements of reactive oxygen species by cyclic hydroxylamine spin probes. Antioxid. Redox Signal. 28 (15), 1433–1443.
Dong, C., Ji, J., Shen, B., Xing, M., Zhang, J., 2018. Enhancement of H_2O_2 decomposition by the co-catalytic effect of WS2 on the Fenton reaction for the synchronous reduction of Cr(VI) and remediation of phenol. Environ. Sci. Technol. 52, 11297–11308.
Dong, Y., Peng, W., Liu, Y., Wang, Z., 2021. Photochemical origin of reactive radicals and halogenated organic substances in natural waters: a review. J. Hazard. Mater. 401, 123884.
Dong, H., Zeng, Q., Sheng, Y., Chen, C., Yu, G., Kappler, A., 2023. Coupled iron cycling and organic matter transformation across redox interfaces. Nat. Rev. Earth Environ. 4, 659–673.
Dorrepaal, E., Toet, S., van Logtestijn, R.S.P., Swart, E., van de Weg, M.J., Callaghan, T. V., Aerts, R., 2009. Carbon respiration from subsurface peat accelerated by climate warming in the subarctic. Nature 460 (7255), 616–619.
Du, H., Cao, Y., Li, Z., Li, L., Xu, H., 2021. Formation and mechanisms of hydroxyl radicals during the oxygenation of sediments in Lake Poyang. China. Water Res. 202, 117442.
Ehrlich, H.L., Newman, D.K., 2008. Geomicrobiology. CRC press.
Finkel, T., Holbrook, N.J., 2000. Oxidants, oxidative stress and the biology of ageing. Nature 408 (6809), 239–247.
Flohé, L., Ötting, F., 1984. [10] Superoxide Dismutase Assays, Methods in Enzymology. Academic Press, pp. 93–104.
Fujii, M., Rose, A.L., Waite, T.D., Omura, T., 2006. Superoxide-mediated dissolution of amorphous ferric oxyhydroxide in seawater. Environ. Sci. Technol. 40, 880–887.
Garg, S., Rose, A.L., Waite, T.D., 2011. Photochemical production of superoxide and hydrogen peroxide from natural organic matter. Geochim. Cosmochim. Acta 75, 4310–4320.
Geiger, S., Lord, G., Tambue, A., 2012. Exponential time integrators for stochastic partial differential equations in 3D reservoir simulation. Comput. Geosci. 16 (2), 323–334.
Gligorovski, S., Strekowski, R., Barbati, S., Vione, D., 2015. Environmental implications of hydroxyl radicals (•OH). Chem. Rev. 115 (24), 13051–13092.
Goldstone, J.V., Pullin, M.J., Bertilsson, S., Voelker, B.M., 2002. Reactions of hydroxyl radical with humic substances: Bleaching, mineralization, and production of bioavailable carbon substrates. Environ. Sci. Technol. 36 (3), 364–372.
Gootman, K.S., González-Pinzón, R., Knapp, J.L.A., Garayburu-Caruso, V., Cable, J.E., 2020. Spatiotemporal variability in transport and reactive processes across a first- to fifth-order fluvial network. Water Resour. Res. 56 (5) e2019WR026303.
Grün, R., 1989. Electron spin resonance (ESR) dating. Quat. Int. 1, 65–109.
Guo, D., Xia, Q., Zeng, Q., Wang, X., Dong, H., 2021. Antibacterial mechanisms of reduced iron-containing smectite-illite clay minerals. Environ. Sci. Technol. 55 (22), 15256–15265.
Halliwell, B., 2006. Reactive species and antioxidants. Redox biology is a fundamental theme of aerobic life. Plant Physiol. 141 (2), 312–322.
Halliwell, B., 2024. Understanding mechanisms of antioxidant action in health and disease. Nat. Rev. Mol. Cell Biol. 25 (1), 13–33.
Hansel, C.M., Diaz, J.M., 2021. Production of extracellular reactive oxygen species by marine biota. Ann. Rev. Mar. Sci. 13, 177–200.
Hansel, C.M., Ferdelman, T.G., Tebo, B.M., 2015. Cryptic cross-linkages among biogeochemical cycles: Novel insights from reactive intermediates. Elements 11 (6), 409–414.
He, W., Liu, Y., Wamer, W.G., Yin, J.J., 2014. Electron spin resonance spectroscopy for the study of nanomaterial-mediated generation of reactive oxygen species. J. Food Drug Anal. 22 (1), 49–63.
He, H., Wu, X., Xian, H., Zhu, J., Yang, Y., Lv, Y., Li, Y., Konhauser, K.O., 2021. An abiotic source of Archean hydrogen peroxide and oxygen that pre-dates oxygenic photosynthesis. Nat. Commun. 12 (1), 6611.
He, H., Wu, X., Zhu, J., Lin, M., Lv, Y., Xian, H., Yang, Y., Lin, X., Li, S., Li, Y., Teng, H., Thiemens, M.H., 2023. A mineral- based origin of Earth's initial hydrogen peroxide and molecular oxygen. Proc. Natl. Acad. Sci. U. S. A. 120 (13), e2221984120.
He, Z., Gao, J., Li, Q., Wei, Z., Zhang, D., Pan, X., 2025. Enhanced oxidation of Mn(II) and as(III) by aerobic granular sludge via ferrous citrate: Key roles of colloidal iron and extracellular superoxide radical. Water Res. 268, 122705.
Hicks Pries, C.E., Castanha, C., Porras, R., Torn, M., 2017. The whole-soil carbon flux in response to warming. Science 355 (6332), 1420–1423.
Hodges, D.M., 2003. Postharvest Oxidative Stress in Horticultural Crops. CRC Press.
Hofmann, A.F., Meysman, F.J.R., Soetaert, K., Middelburg, J.J., 2008. A step-by-step procedure for pH model construction in aquatic systems. Biogeosciences 5 (1), 227–251.
Hopwood, M.J., Rapp, I., Schlosser, C., Achterberg, E.P., 2017. Hydrogen peroxide in deep waters from the Mediterranean Sea, South Atlantic and South Pacific Oceans. Sci. Rep. 7 (1), 43436.
Hu, B., Zhang, P., Liu, H., Yuan, S., 2022. Quantification of the influence of citrate/Fe(II) molar ratio on hydroxyl radical production and pollutant degradation during Fe(II)-catalyzed O_2 and H_2O_2 oxidation processes. Int. J. Environ. Res. Public Health 19 (19), 12977.
Hu, D., Zeng, Q., Zhu, J., He, C., Shi, Q., Dong, H., 2023. Promotion of humic acid transformation by abiotic and biotic fe redox cycling in nontronite. Environ. Sci. Technol. 57 (48), 19760–19771.
Huang, H., Ji, X.B., Cheng, L.Y., Zhao, F.J., Wang, P., 2021a. Free radicals produced from the oxidation of ferrous sulfides promote the remobilization of cadmium in paddy soils during drainage. Environ. Sci. Technol. 55 (14), 9845–9853.
Huang, J., Jones, A., Waite, T.D., Chen, Y., Huang, X., Rosso, K.M., Kappler, A., Mansor, M., Tratnyek, P.G., Zhang, H., 2021b. Fe(II) redox chemistry in the environment. Chem. Rev. 121 (13), 8161–8233.
Huang, D., Chen, N., Zhu, C., Sun, H., Fang, G., Zhou, D., 2023. Dynamic production of hydroxyl radicals during the flooding–drainage process of paddy soil: An in situ column study. Environ. Sci. Technol. 57 (43), 16340–16347.
Hug, S.J., Leupin, O., 2003. Iron-catalyzed oxidation of arsenic(III) by oxygen and by hydrogen peroxide: pH-dependent formation of oxidants in the Fenton reaction. Environ. Sci. Technol. 37 (12), 2734–2742.
Jia, M., Bian, X., Yuan, S., 2017. Production of hydroxyl radicals from Fe(II) oxygenation induced by groundwater table fluctuations in a sand column. Sci. Total Environ. 584-585, 41–47.
Kakkar, P., Das, B., Viswanathan, P., 1984. A modified spectrophotometric assay of superoxide dismutase. Indian J. Biochem. Biophys. 21, 130–132.
Kaplan, D.I., Xu, C., Huang, S., Lin, Y., Tolic, N., Roscioli-Johnson, K.M., Santschi, P.H., Jaffe, P.R., 2016. Unique organic matter and microbial properties in the rhizosphere of a wetland soil. Environ. Sci. Technol. 50 (8), 4169–4177.
Kappler, A., Bryce, C., Mansor, M., Lueder, U., Byrne, J.M., Swanner, E.D., 2021. An evolving view on biogeochemical cycling of iron. Nat. Rev. Microbiol. 19 (6), 360–374.
Khan, N., Seshadri, B., Bolan, N., Saint, C.P., Kirkham, M.B., Chowdhury, S., Yamaguchi, N., Lee, D.Y., Li, G., Kunhikrishnan, A., Qi, F., Karunanithi, R., Qiu, R., Zhu, Y.G., Syu, C.H., 2016. Chapter one - root iron plaque on wetland plants as a dynamic pool of nutrients and contaminants. In: Sparks, D.L. (Ed.), Advances in Agronomy. Academic Press, pp. 1–96.
King, D.W., Cooper, W.J., Rusak, S.A., Peake, B.M., Kiddle, J.J., O'Sullivan, D.W., Melamed, M.L., Morgan, C.R., Theberge, S.M., 2007. Flow injection analysis of H_2O_2 in natural waters using acridinium ester chemiluminescence: method development and optimization using a kinetic model. Anal. Chem. 79 (11), 4169–4176.
Kinsela, A.S., Jones, A.M., Bligh, M.W., Pham, A.N., Collins, R.N., Harrison, J.J., Wilsher, K.L., Payne, T.E., Waite, T.D., 2016. Influence of dissolved silicate on rates of Fe(II) oxidation. Environ. Sci. Technol. 50 (21), 11663–11671.
Klupfel, L., Piepenbrock, A., Kappler, A., Sander, M., 2014. Humic substances as fully regenerable electron acceptors in recurrently anoxic environments. Nat. Geosci. 7 (3), 195–200.
Kögel-Knabner, I., Amelung, W., Cao, Z., Fiedler, S., Frenzel, P., Jahn, R., Kalbitz, K., Kölbl, A., Schloter, M., 2010. Biogeochemistry of paddy soils. Geoderma 157 (1–2), 1–14.
Kono, Y., 1978. Generation of superoxide radical during autoxidation of hydroxylamine and an assay for superoxide dismutase. Arch. Biochem. Biophys. 186 (1), 189–195.
Kräutle, S., Knabner, P., 2007. A reduction scheme for coupled multicomponent transport-reaction problems in porous media: Generalization to problems with heterogeneous equilibrium reactions. Water Resour. Res. 43 (3), W03429.

Krumova, K., Cosa, G., 2016. Overview of Reactive Oxygen Species.
Kwan, W.P., Voelker, B.M., 2002. Decomposition of hydrogen peroxide and organic compounds in the presence of dissolved iron and ferrihydrite. Environ. Sci. Technol. 36 (7), 1467–1476.
Lam, S.H., 1993. Using CSP to understand complex chemical kinetics. Combust. Sci. Technol. 89 (5–6), 375–404.
Lam, S.H., Goussis, D.A., 1994. The CSP method for simplifying kinetics. Int. J. Chem. Kinet. 26 (4), 461–486.
Latch, D.E., McNeill, K., 2006. Microheterogeneity of singlet oxygen distributions in irradiated humic acid solutions. Science 311 (5768), 1743–1747.
Learman, D.R., Voelker, B.M., Vazquez-Rodriguez, A.I., Hansel, C.M., 2011. Formation of manganese oxides by bacterially generated superoxide. Nat. Geosci. 4 (2), 95–98.
Lee, J.K., Walker, K.L., Han, H.S., Kang, J., Prinz, F.B., Waymouth, R.M., Nam, H.G., Zare, R.N., 2019. Spontaneous generation of hydrogen peroxide from aqueous microdroplets. Proc. Natl. Acad. Sci. U. S. A. 116 (39), 19294–19298.
Lee, J.K., Han, H.S., Chaikasetsin, S., Marron, D.P., Waymouth, R.M., Prinz, F.B., Zare, R. N., 2020. Condensing water vapor to droplets generates hydrogen peroxide. Proc. Natl. Acad. Sci. U. S. A. 117 (49), 30934–30941.
Lefticariu, L., Pratt, L.A., LaVerne, J.A., Schimmelmann, A., 2010. Anoxic pyrite oxidation by water radiolysis products — a potential source of biosustaining energy. Earth Planet. Sci. Lett. 292 (1–2), 57–67.
Li, L., Maher, K., Navarre-Sitchler, A., Druhan, J., Meile, C., Lawrence, C., Moore, J., Perdrial, J., Sullivan, P., Thompson, A., Jin, L., Bolton, E.W., Brantley, S.L., Dietrich, W.E., Mayer, K.U., Steefel, C.I., Valocchi, A., Zachara, J., Kocar, B., McIntosh, J., Tutolo, B.M., Kumar, M., Sonnenthal, E., Bao, C., Beisman, J., 2017. Expanding the role of reactive transport models in critical zone processes. Earth Sci. Rev. 165, 280–301.
Li, C., Zhang, Y., Zheng, Y., Shi, C., Lu, Y., Zhang, Y., Yuan, S., 2024. Contaminant transformation during sediment oxygenation: Temporal variation of oxidation mechanisms mediated by hydroxyl radicals and aerobic microbes. Sci. Total Environ. 919, 170855.
Liao, W., Ye, Z., Yuan, S., Cai, Q., Tong, M., Qian, A., Cheng, D., 2019. Effect of coexisting Fe(III) (oxyhydr)oxides on Cr(VI) reduction by Fe(II)-bearing clay minerals. Environ. Sci. Technol. 53, 13767–13775.
Lin, S., Xu, L., Chi Wang, A., Wang, Z.L., 2020. Quantifying electron-transfer in liquid-solid contact electrification and the formation of electric double-layer. Nat. Commun. 11 (1), 399.
Liu, J., Zhu, K., Zhang, C., Zhang, X., Chen, N., Jia, H., 2022. Microscale spatiotemporal variation and generation mechanisms of reactive oxygen species in the rhizosphere of ryegrass: coupled biotic-abiotic processes. Environ. Sci. Technol. 56 (22), 16483–16493.
Liu, F., Wang, Z., Liu, J., Latif, J., Qin, J., Yang, H., Jiang, W., Deng, Y., Yang, K., Ni, Z., Ding, Y., Xie, J., Wang, Y., Jia, H., 2024a. Seasonal and spatial fluctuations of reactive oxygen species in riparian soils and their contributions on organic carbon mineralization. Environ. Sci. Technol. 58 (16), 7066–7077.
Liu, J., Zhu, C., Zhu, F., Sun, H., Wang, J., Fang, G., Zhou, D., 2024b. Strong substance exchange at paddy soil-water interface promotes nonphotochemical formation of reactive oxygen species in overlying water. Environ. Sci. Technol. 58 (17), 7403–7414.
Liu, Y., Zhang, Y., Chen, G., Li, Y., Zeng, Q., Hu, J., Hu, D., Dong, H., 2024c. Molecular transformation of petroleum compounds by hydroxyl radicals produced upon oxidation of reduced nontronite. Geochim. Cosmochim. Acta 371, 31–51.
Ma, S., Tong, M., Yuan, S., Liu, H., 2019. Responses of the microbial community structure in Fe(II)-bearing sediments to oxygenation: the role of reactive oxygen species. ACS Earth Space Chem. 3 (5), 738–747.
Meng, F.L., Zhang, X., Hu, Y., Sheng, G.P., 2023. New barrier role of iron plaque: Producing interfacial hydroxyl radicals to degrade rhizosphere pollutants. Environ. Sci. Technol. 58 (1), 795–804.
Miller, C.J., Rose, A.L., Waite, T.D., 2013. Hydroxyl radical production by H_2O_2-mediated oxidation of Fe(II) complexed by Suwannee River fulvic acid under circumneutral freshwater conditions. Environ. Sci. Technol. 47 (2), 829–835.
Miller, C.J., Rose, A.L., Waite, T.D., 2016. Importance of iron complexation for Fenton-mediated hydroxyl radical production at circumneutral pH. Front. Mar. Sci. 3 (134).
Miller, C.J., Wadley, S., Waite, T.D., 2018. Fenton, photo-Fenton and Fenton-like processes. In "Advanced Oxidation Processes for Water Treatment: Fundamentals and applications", Mihaela J. Stefan (Ed.), IWA Press (ISBN13: 9781780407180, eISBN: 9781780407197). Chapter 7, 297–323.
Mopper, K., Zhou, X., 1990. Hydroxyl radical photoproduction in the sea and its potential impact on marine processes. Science 250 (4981), 661–664.
Morgan, J.J., 2005. Kinetics of reaction between O_2 and Mn(II) species in aqueous solutions. Geochim. Cosmochim. Acta 69 (1), 35–48.
Nandi, A., Chatterjee, I., 1988. Assay of superoxide dismutase activity in animal tissues. J. Biosci. 13, 305–315.
Nie, J., Ren, Z., Xu, L., Lin, S., Zhan, F., Chen, X., Wang, Z.L., 2020. Probing contact-electrification-induced electron and ion transfers at a liquid–solid interface. Adv. Mater. 32 (2), 1905696.
Nishinaka, Y., Aramaki, Y., Yoshida, H., Masuya, H., Sugawara, T., Ichimori, Y., 1993. A New Sensitive Chemiluminescence Probe, L-012, for measuring the production of Superoxide Anion by Cells. Biochem. Biophys. Res. Commun. 193 (2), 554–559.
Niyuhire, E., Yuan, S., Liao, W., Zhu, J., Liu, X., Xie, W., Qian, A., 2019. Sulfide drives hydroxyl radicals production in oxic ferric oxyhydroxides environments. Chemosphere 234, 450–460.
Niyuhire, E., Zhou, C., Hu, B., Cai, Q., Yuan, S., 2022. Sulfide perturbation of NOM-bearing oxic environments induces dark •OH production. Chem. Geol. 613, 121147.
Nosaka, Y., Nosaka, A.Y., 2017. Generation and detection of reactive oxygen species in photocatalysis. Chem. Rev. 117 (17), 11302–11336.
Page, S.E., Sander, M., Arnold, W.A., McNeill, K., 2012. Hydroxyl radical formation upon oxidation of reduced humic acids by oxygen in the dark. Environ. Sci. Technol. 46 (3), 1590–1597.
Page, S.E., Kling, G.W., Sander, M., Harrold, K.H., Logan, J.R., McNeill, K., Cory, R.M., 2013. Dark formation of hydroxyl radical in Arctic soil and surface waters. Environ. Sci. Technol. 47 (22), 12860–12867.
Pan, Y., Zheng, X., Zhao, G., Rao, Z., Yu, W., Chen, B., Chu, C., 2023. Water vapor condensation on iron minerals spontaneously produces hydroxyl radical. Environ. Sci. Technol. 57 (23), 8610–8616.
Petasne, R.G., Zika, R.G., 1987. Fate of superoxide in coastal sea water. Nature 325 (6104), 516–518.
Philippot, L., Raaijmakers, J.M., Lemanceau, P., van der Putten, W.H., 2013. Going back to the roots: the microbial ecology of the rhizosphere. Nat. Rev. Microbiol. 11 (11), 789–799.
Plummer, S., Taylor, A.E., Harvey, E.L., Hansel, C.M., Diaz, J.M., 2019. Dynamic regulation of extracellular superoxide production by the coccolithophore *Emiliania Huxleyi* (CCMP 374). Front. Microb. 10, 1546.
Prinn, R., Huang, J., Weiss, R., Cunnold, D., Fraser, P., Simmonds, P., McCulloch, A., Harth, C., Salameh, P., O'doherty, S., 2001. Evidence for substantial variations of atmospheric hydroxyl radicals in the past two decades. Science 292 (5523), 1882–1888.
Prommer, H., Sun, J., Kocar, B.D., 2019. Using reactive transport models to quantify and predict groundwater quality. Elements 15 (2), 87–92.
Prónai, L., Nakazawa, H., Ichimori, K., Saigusa, Y., Ohkubo, T., Hiramatsu, K., Arimori, S., Fehér, J., 1992. Time course of superoxide generation by leukocytes—the MCLA chemiluminescence system. Inflammation 16 (5), 437–450.
Qi, J., Wang, X., Lin, Z., Zhao, J., Hu, C., Qu, J., 2024. Algae promotes the biogenic oxidation of Mn(II) by accelerated extracellular superoxide production. Water Res. 261, 122063.
Qian, A., Yuan, S., Xie, S., Tong, M., Zhang, P., Zheng, Y., 2019. Oxidizing capacity of iron electrocoagulation systems for refractory organic contaminant transformation. Environ. Sci. Technol. 53 (21), 12629–12638.
Ratasuk, N., Nanny, M.A., 2007. Characterization and quantification of reversible redox sites in humic substances. Environ. Sci. Technol. 41 (22), 7844–7850.
Remucal, C.K., Sedlak, D.L., 2011. The role of iron coordination in the production of reactive oxidants from ferrous iron oxidation by oxygen and hydrogen peroxide. Aquatic redox chemistry. ACS Publications 177–197.
Rhee, S.G., Chang, T.-S., Jeong, W., Kang, D., 2010. Methods for detection and measurement of hydrogen peroxide inside and outside of cells. Mol. Cells 29, 539–549.
Roelandt, C., Goddéris, Y., Bonnet, M.P., Sondag, F., 2010. Coupled modeling of biospheric and chemical weathering processes at the continental scale. Glob. Biogeochem. Cycle 24 (2), GB2004.
Rose, A.L., Waite, T.D., 2002. Kinetic model for Fe(II) oxidation in seawater in the absence and presence of natural organic matter. Environ. Sci. Technol. 36 (3), 433–444.
Rose, A.L., Waite, T.D., 2005. Reduction of organically complexed ferric iron by superoxide in a simulated natural water. Environ. Sci. Technol. 39 (8), 2645–2650.
Rose, A.L., Salmon, T.P., Lukondeh, T., Neilan, B.A., Waite, T.D., 2005. Use of superoxide as an electron shuttle for iron acquisition by the marine cyanobacterium lyngbya majuscula. Environ. Sci. Technol. 39 (10), 3708–3715.
Rose, A.L., Moffett, J.W., Waite, T.D., 2008a. Determination of superoxide in seawater using 2-methyl-6-(4-methoxyphenyl)-3,7- dihydroimidazo[1,2-a]pyrazin-3(7H)-one chemiluminescence. Anal. Chem. 80 (4), 1215–1227.
Rose, A.L., Webb, E.A., Waite, T.D., Moffett, J.W., 2008b. Measurement and Implications of Nonphotochemically Generated Superoxide in the Equatorial Pacific Ocean. Environ. Sci. Technol. 42, 2387–2393.
Rosso, K.M., Morgan, J.J., 2002. Outer-sphere electron transfer kinetics of metal ion oxidation by molecular oxygen. Geochim. Cosmochim. Acta 66 (24), 4223–4233.
Savee, J.D., Papajak, E., Rotavera, B., Huang, H., Eskola, A.J., Welz, O., Sheps, L., Taatjes, C.A., Zador, J., Osborn, D.L., 2015. Direct observation and kinetics of a hydroperoxyalkyl radical (QOOH). Science 347 (6222), 643–646.
Schaefer, C.E., Ho, P., Gurr, C., Berns, E., Werth, C., 2017. Abiotic dechlorination of chlorinated ethenes in natural clayey soils: Impacts of mineralogy and temperature. J. Contam. Hydrol. 206, 10–17.
Schaefer, C.E., Ho, P., Berns, E., Werth, C., 2018. Mechanisms for abiotic dechlorination of trichloroethene by ferrous minerals under oxic and anoxic conditions in natural sediments. Environ. Sci. Technol. 52 (23), 13747–13755.
Schieber, M., Chandel, N.S., 2014. ROS function in redox signaling and oxidative stress. Curr. Biol. 24 (10), R453–R462.
Schneider, R.J., Roe, K.L., Hansel, C.M., Voelker, B.M., 2016. Species-Level Variability in Extracellular Production Rates of Reactive Oxygen Species by Diatoms. Front, Chem, p. 4.
Schoonen, M.A., Cohn, C.A., Roemer, E., Laffers, R., Simon, S.R., Riordan, O., 2006. Mineral-induced formation of reactive oxygen species. Rev. Mineral. Geochem. 64, 179.
Sekar, R., DiChristina, T.J., 2014. Microbially driven Fenton reaction for degradation of the widespread environmental contaminant 1,4-dioxane. Environ. Sci. Technol. 48 (21), 12858–12867.
Shaked, Y., Harris, R., Klein-Kedem, N., 2010. Hydrogen peroxide photocycling in the Gulf of Aqaba. Red sea. Environ. Sci. Technol. 44 (9), 3238–3244.
Sheng, Y., Hu, J., Kukkadapu, R., Guo, D., Zeng, Q., Dong, H., 2023. Inhibition of extracellular enzyme activity by reactive oxygen species upon oxygenation of reduced iron-bearing minerals. Environ. Sci. Technol. 57 (8), 3425–3433.

Song, Y., Buettner, G.R., 2010. Thermodynamic and kinetic considerations for the reaction of semiquinone radicals to form superoxide and hydrogen peroxide. Free Radic. Biol. Med. 49 (6), 919–962.
Stone, J., Edgar, J.O., Gould, J.A., Telling, J., 2022. Tectonically-driven oxidant production in the hot biosphere. Nat. Commun. 13 (1), 4529.
Su, Y., Song, H., Lv, Y., 2019. Recent advances in chemiluminescence for reactive oxygen species sensing and imaging analysis. Microchem. J. 146, 83–97.
Sun, Z., Huang, M., Liu, C., Fang, G., Chen, N., Zhou, D., Gao, J., 2020. The formation of •OH with Fe-bearing smectite clays and low-molecular-weight thiols: Implication of as(III) removal. Water Res. 174, 115631.
Sutherland, K.M., Wankel, S.D., Hansel, C.M., 2020. Dark biological superoxide production as a significant flux and sink of marine dissolved oxygen. Proc. Natl. Acad. Sci. U. S. A. 117 (7), 3433–3439.
Swanner, E.D., Mloszewska, A.M., Cirpka, O.A., Schoenberg, R., Konhauser, Kurt O., Kappler, A., 2015. Modulation of oxygen production in Archaean oceans by episodes of Fe(II) toxicity. Nat. Geosci. 8 (2), 126–130.
Szymczak, R., Waite, T.D., 1991. Photochemical activity in waters of the Great Barrier Reef. Estuar. Coast. Shelf Sci. 33, 605–622.
Taverne, Y.J., Merkus, D., Bogers, A.J., Halliwell, B., Duncker, D.J., Lyons, T.W., 2018. Reactive oxygen species: Radical factors in the evolution of animal life: a molecular timescale from Earth's earliest history to the rise of complex life. BioEssays 40 (3), 1700158.
Tolar, B.B., Powers, L.C., Miller, W.L., Wallsgrove, N.J., Popp, B.N., Hollibaugh, J.T., 2016. Ammonia oxidation in the ocean can be inhibited by nanomolar concentrations of hydrogen peroxide. Front. Mar. Sci. 3, 237.
Tong, M., Yuan, S., Ma, S., Jin, M., Liu, D., Cheng, D., Liu, X., Gan, Y., Wang, Y., 2016. Production of abundant hydroxyl radicals from oxygenation of subsurface sediments. Environ. Sci. Technol. 50 (1), 214–221.
Tong, M., Zhao, Y., Sun, Q., Li, P., Liu, H., Yuan, S., 2022. Fe(II) oxygenation inhibits bacterial Mn(II) oxidation by *P. Putida* MnB1 in groundwater under O_2-perturbed conditions. J. Hazard. Mater. 435, 128972.
Trusiak, A., Treibergs, L.A., Kling, G.W., Cory, R.M., 2018. The role of iron and reactive oxygen species in the production of CO_2 in arctic soil waters. Geochim. Cosmochim. Acta 224, 80–95.
Van Erk, M.R., Bourceau, O.M., Moncada, C., Basu, S., Hansel, C.M., De Beer, D., 2023. Reactive oxygen species affect the potential for mineralization processes in permeable intertidal flats. Nat. Commun. 14 (1), 938.
Waite, T.D., Sawyer, D.T., Zafiriou, O.C., 1988. Panel 1: Oceanic reactive chemical transients. Appl. Geochem. 3 (1), 9–17.
Wang, D., Zhao, L., Ma, H., Zhang, H., Guo, L.-H., 2017a. Quantitative analysis of reactive oxygen species photogenerated on metal oxide nanoparticles and their bacteria toxicity: the role of superoxide radicals. Environ. Sci. Technol. 51 (17), 10137–10145.
Wang, X., Dong, H., Zeng, Q., Xia, Q., Zhang, L., Zhou, Z., 2017b. Reduced iron-containing clay minerals as antibacterial agents. Environ. Sci. Technol. 51 (13), 7639–7647.
Wang, Y., Wang, H., He, J.S., Feng, X., 2017c. Iron-mediated soil carbon response to water-table decline in an alpine wetland. Nat. Commun. 8, 15972.
Wang, Q., Hu, Y., Xie, H., Yang, Z., 2018. Constructed wetlands: a review on the role of radial oxygen loss in the rhizosphere by macrophytes. Water 10 (6), 678.
Wang, P., Li, J., An, P., Yan, Z., Xu, Y., Pu, S., 2023. Enhanced delivery of remedial reagents in low-permeability aquifers through coupling with groundwater circulation well. J. Hydrol. 618, 129260.
Wang, P., Li, J., An, P., Yang, B., Hou, D., Pu, S., 2024. Understanding the dilemmas and breakdown of the reactive migration of in situ groundwater injection reagents from an environmental geology perspective. Crit. Rev. Environ. Sci. Technol. 54 (9), 747–770.
Wei, X., Zhu, Z., Wei, L., Wu, J., Ge, T., 2019. Biogeochemical cycles of key elements in the paddy-rice rhizosphere: Microbial mechanisms and coupling processes. Rhizosphere 10, 100145.
Wei, Y., Chen, Y., Cao, X., Xiang, M., Huang, Y., Li, H., 2024. A critical review of groundwater table fluctuation: Formation, effects on multifields, and contaminant behaviors in a soil and aquifer system. Environ. Sci. Technol. 58 (5), 2185–2203.
Wood, P.M., 1988. The potential diagram for oxygen at pH 7. Biochem. J. 253 (1), 287–289.
Wu, M.Z., Reynolds, D.A., Prommer, H., Fourie, A., Thomas, D.G., 2012. Numerical evaluation of voltage gradient constraints on electrokinetic injection of amendments. Adv. Water Resour. 38, 60–69.
Wu, X., Zhu, J., He, H., Xian, H., Yang, Y., Ma, L., Liang, X., Lin, X., Li, S., Konhauser, K. O., Li, Y., 2023. Geodynamic oxidation of Archean terrestrial surfaces. Commun. Earth Environ. 4 (1), 132.
Xia, Y., Li, J., Zhang, Y., Yin, Y., Chen, B., Jiang, G., Zare, R., 2023. Contact between water vapor and silicate surface causes abiotic formation of reactive oxygen species in an anoxic atmosphere. Proc. Natl. Acad. Sci. U. S. A. 120 (30), e2302014120.
Xie, W., Yuan, S., Tong, M., Ma, S., Liao, W., Zhang, N., Chen, C., 2020. Contaminant degradation by •OH during sediment oxygenation: Dependence on Fe(II) species. Environ. Sci. Technol. 54 (5), 2975–2984.
Xie, W., Zhang, P., Liao, W., Tong, M., Yuan, S., 2021. Ligand-enhanced electron utilization for trichloroethylene degradation by ·OH during sediment oxygenation. Environ. Sci. Technol. 55 (10), 7044–7051.
Xing, R., Yang, X., Sun, H., Ye, X., Liao, H., Qin, S., Chen, Z., Zhou, S., 2022. Extensive production and evolution of free radicals during composting. Bioresour. Technol. 359, 127491.
Xu, C., Zi, Y., Wang, A.C., Zou, H., Dai, Y., He, X., Wang, P., Wang, Y., Feng, P., Li, D., Wang, Z.L., 2018. On the electron-transfer mechanism in the contact-electrification effect. Adv. Mater. 30 (15), 1706790.
Yeh, G.-T., Fang, Y., Zhang, F., Sun, J., Li, Y., Li, M.-H., Siegel, M.D., 2009. Numerical modeling of coupled fluid flow and thermal and reactive biogeochemical transport in porous and fractured media. Comput. Geosci. 14 (1), 149–170.
Yu, G.-H., Kuzyakov, Y., 2021. Fenton chemistry and reactive oxygen species in soil: Abiotic mechanisms of biotic processes, controls and consequences for carbon and nutrient cycling. Earth Sci. Rev. 214, 103525.
Yu, C., Zhang, Y., Lu, Y., Qian, A., Zhang, P., Cui, Y., Yuan, S., 2021a. Mechanistic insight into humic acid-enhanced hydroxyl radical production from Fe(II)-bearing clay mineral oxygenation. Environ. Sci. Technol. 55 (19), 13366–13375.
Yu, H., Zhang, P., Liu, J., Zheng, Y., Mustapha, N.A., 2021b. Effects of low-molecular-weight organic acids/thiols on hydroxyl radical production from natural siderite oxidation. Chem. Geol. 584, 120537.
Yu, C., Lu, Y., Zhang, Y., Qian, A., Zhang, P., Tong, M., Yuan, S., 2022. Significant contribution of solid organic matter for hydroxyl radical production during oxygenation. Environ. Sci. Technol. 56 (16), 11878–11887.
Yu, W., Zheng, X., Tan, M., Wang, J., Wu, B., Ma, J., Pan, Y., Chen, B., Chu, C., 2024. Field quantification of hydroxyl radicals by flow-injection chemiluminescence analysis with a portable device. Environ. Sci. Technol. 58 (6), 2808–2816.
Yu, W., Ma, J., Tan, M., Wang, J., Zheng, X., Wu, B., Chen, B., Chu, C., 2025. Visualizing hydrogen peroxide diffusion in soils with precipitation-based fluorescent probe. Environ. Sci. Technol. 59 (1), 545–552.
Yuan, J., Shiller, A.M., 2004. Hydrogen peroxide in deep waters of the North Pacific Ocean. Geophys. Res. Lett. 31 (1), L01310.
Yuan, X., Nico, P.S., Huang, X., Liu, T., Ulrich, C., Williams, K.H., Davis, J.A., 2017. Production of hydrogen peroxide in groundwater at Rifle. Colorado. Environ. Sci. Technol. 51 (14), 7881–7891.
Yuan, S., Liu, X., Liao, W., Zhang, P., Wang, X., Tong, M., 2018. Mechanisms of electron transfer from structrual Fe(II) in reduced nontronite to oxygen for production of hydroxyl radicals. Geochim. Cosmochim. Acta 223, 422–436.
Yuan, X., Liu, T., Fox, P., Bhattacharyya, A., Dwivedi, D., Williams, K.H., Davis, J.A., Waite, T.D., Nico, P.S., 2022. Production of hydrogen peroxide in an intra-meander hyporheic zone at East River. Colorado. Sci Rep. 12 (1), 712.
Zeng, Q., Dong, H., Wang, X., Yu, T., Cui, W., 2017. Degradation of 1, 4-dioxane by hydroxyl radicals produced from clay minerals. J. Hazard. Mater. 331, 88–98.
Zeng, Q., Dong, H., Wang, X., 2019. Effect of ligands on the production of oxidants from oxygenation of reduced Fe-bearing clay mineral nontronite. Geochim. Cosmochim. Acta 251, 136–156.
Zeng, Q., Wang, X., Liu, X., Huang, L., Hu, J., Chu, R., Tolic, N., Dong, H., 2020. Mutual interactions between reduced Fe-bearing clay minerals and humic acids under dark, oxygenated conditions: hydroxyl radical generation and humic acid transformation. Environ. Sci. Technol. 54 (23), 15013–15023.
Zhang, L., Jun, Y.S., 2018. The role of Fe-bearing phyllosilicates in DTPMP degradation under high-temperature and high-pressure conditions. Environ. Sci. Technol. 52 (16), 9522–9530.
Zhang, P., Yuan, S., 2017. Production of hydroxyl radicals from abiotic oxidation of pyrite by oxygen under circumneutral conditions in the presence of low-molecular-weight organic acids. Geochim. Cosmochim. Acta 218, 153–166.
Zhang, P., Yuan, S., Liao, P., 2016a. Mechanisms of hydroxyl radical production from abiotic oxidation of pyrite under acidic conditions. Geochim. Cosmochim. Acta 172, 444–457.
Zhang, T., Hansel, C.M., Voelker, B.M., Lamborg, C.H., 2016b. Extensive dark biological production of reactive oxygen species in brackish and freshwater ponds. Environ. Sci. Technol. 50 (6), 2983–2993.
Zhang, P., Huang, W., Ji, Z., Zhou, C., Yuan, S., 2018. Mechanisms of hydroxyl radicals production from pyrite oxidation by hydrogen peroxide: Surface versus aqueous reactions. Geochim. Cosmochim. Acta 238, 394–410.
Zhang, N., Bu, X., Li, Y., Zhang, Y., Yuan, S., Wen, Z., Tong, M., Lin, L., 2020a. Water table fluctuations regulate hydrogen peroxide production and distribution in unconfined aquifers. Environ. Sci. Technol. 54 (8), 4942–4951.
Zhang, P., Yuan, S., Chen, R., Bu, X., Tong, M., Huang, Q., 2020b. Oxygenation of acid sulfate soils stimulates CO_2 emission: Roles of acidic dissolution and hydroxyl radical oxidation. Chem. Geol. 533, 119437.
Zhang, S., Lv, J., Han, R., Wang, Z., Christie, P., Zhang, S., 2021. Sustained production of superoxide radicals by manganese oxides under ambient dark conditions. Water Res. 196, 117034.
Zhang, X., Jia, Q., Deng, J., Wu, F., Huang, L.Z., 2022a. Interaction between green rust and tribromophenol under anoxic, oxic and anoxic-to-oxic conditions: Adsorption, desorption and oxidative degradation. Water Res. 217, 118398.
Zhang, Y., Zhang, N., Qian, A., Yu, C., Zhang, P., Yuan, S., 2022b. Effect of C/Fe molar ratio on H_2O_2 and •OH production during oxygenation of Fe(II)-humic acid coexisting systems. Environ. Sci. Technol. 56 (18), 13408–13418.
Zhang, P., Liu, J., Yu, H., Cheng, D., Liu, H., Yuan, S., 2023a. Kinetic models for hydroxyl radical production and contaminant removal during soil/sediment oxygenation. Water Res. 240, 120071.
Zhang, Y., Zhang, N., Yu, C., Liu, H., Yuan, S., 2023b. ROS production upon groundwater oxygenation: Implications of oxidative capacity during groundwater abstraction and discharging. J. Hydrol. 620, 129551.
Zhang, N., Liu, Y., Wan, Z., Zhang, Y., Xie, W., Zhang, P., Tong, M., Yuan, S., 2024a. Dependence of biotic and abiotic H_2O_2 and •OH production on the redox conditions and compositions of sediment during oxygenation. Environ. Sci. Technol. 58 (8), 3849–3857.
Zhang, P., Zhang, W., Yu, H., Chen, R., Liu, Y., Tian, Y., Yuan, S., 2024b. Fe(III) oxyhydroxides mediated electron transfer from thiols to O_2 for hydroxyl radical production. Chem. Geol. 648, 121962.

Zhao, Y., Xiang, W., Huang, C., Liu, Y., Tan, Y., 2021. Production of hydroxyl radicals following water-level drawdown in peatlands: a new induction mechanism for enhancing laccase activity in carbon cycling. Soil Biol. Biochem. 156, 108241.
Zhao, G., Wu, B., Zheng, X., Chen, B., Kappler, A., Chu, C., 2022. Tide-triggered production of reactive oxygen species in coastal soils. Environ. Sci. Technol. 56 (16), 11888–11896.
Zheng, X., Wu, B., Zhou, C., Liu, T., Wang, Y., Zhao, G., Chen, B., Chu, C., 2023. Sunlight-driven production of reactive oxygen species from natural iron minerals: quantum yield and wavelength dependence. Environ. Sci. Technol. 57 (2), 1177–1185.
Zheng, Y., Tan, Y., Wan, Z., Zhang, P., Li, X., Yuan, S., 2025. Carbon isotope fractionation of dissolved organic matter due to •OH-based oxidation. Environ. Sci. Technol. 59 (18), 9104–9112.
Zhou, M., Diwu, Z., Panchuk-Voloshina, N., Haugland, R.P., 1997. A stable nonfluorescent derivative of resorufin for the fluorometric determination of trace hydrogen peroxide: applications in detecting the activity of phagocyte NADPH oxidase and other oxidases. Anal. Biochem. 253 (2), 162–168.
Zhou, Z., Yu, T., Dong, H., Huang, L., Chu, R.K., Tolic, N., Wang, X., Zeng, Q., 2019. Chemical oxygen demand (COD) removal from bio-treated coking wastewater by hydroxyl radicals produced from a reduced clay mineral. Appl. Clay Sci. 180, 105199.
Zika, R.G., Milne, P.J., Zafiriou, O.C., 1993. Photochemical studies of the eastern Caribbean: An introductory overview. J. Geophys. Res.-Oceans 98 (C2), 2223–2232.
Zinser, E.R., 2018. The microbial contribution to reactive oxygen species dynamics in marine ecosystems. Environ. Microbiol. Rep. 10, 412–427.